UNIVERSITÀ
DEGLI STUDI
DI PADOVA

Università degli Studi di Padova
Dipartimento di Ingegneria Civile, Edile e Ambientale (ICEA)
Department of Civil, Environmental and Architectural Engineering

CORSO DI DOTTORATO DI RICERCA IN SCIENZE DELL'INGEGNERIA CIVILE, AMBIENTALE E DELL'ARCHITETTURA
CURRICOLO: Rischio, vulnerabilità, ambiente, salute e territorio
XXXIV CICLO

The Transport, Diffusion and Retention of Floating Particles within Emergent Vegetation

Tesi redatta con il contributo finanziario del China Scholarship Council (CSC)

Coordinatore: Prof. Carmelo Maiorana
Supervisore: Prof. Andrea Defina
Co-Supervisore: Prof. Paolo Peruzzo

Dottorando: Wei Shi

The Transport, Diffusion and Retention of Floating Particles within Emergent Vegetation

Wei Shi
Supervisors: **Andrea Defina, Paolo Peruzzo**

November 29, 2021

Acknowledgments

Time flies when you're having fun! I have been in Italy for three years, the tension and nervousness when I first met Andrea and Paolo are still vivid, as if it was yesterday. Now I have gradually become accustomed to the pace of life and work here, and gradually like it. I worried about the terrible epidemic in Italy, and I also cheered for the Italian Football Team winning the European Cup. The people here are really cute, humorous, gentleman, optimistic, kind, and friendly! I have received kindly help from many people, here I mainly want to thank a few people.

First of all, I would like to express my sincere gratitude to my supervisor, Professor Andrea Defina, for his continuous support, patience, kindness, and immense wisdom to help me successfully complete the thesis. He is so smart, intelligent, experienced and knowledgeable that he can always point to the core of the research and point out the solution! We don't talk too much, but his comments and revisions to the manuscript can always provide a further insight, make me clear, and raise the level of the paper, which benefit me a lot and deserve my further reading and studying.

I am also grateful and indebted to my respected co-supervisor Dr. Paolo Peruzzo, for his patient and almost hands-on guidance on my research over the three years, for his tolerance and understanding of some academic mistakes I made during the three years, for his equal and respectful dialogue and discussion with me, and for his care and help to my life in Italy! I learned a lot from him! It was happy and fulfilled for me to work with him three years.

I would like to thanks to Enrica Belluco, Carlo Salmaso, and Roberto Frizzerin for their contribution to the experimental investigations, and thanks to my colleagues Teng Ma, JieTuo Wang, Qing Wang, Tian Xie, Liang Geng, Zhicheng Yang, Davide Tognin, Leonardo Costa, and Luigi Di Micco for their help and care in my study life in Italy.

Finally, I would like to thanks to my country and my parents for their financial and spiritual support for me to study for a PhD degree abroad!

Wei Shi
Padova, November 29, 2021

Abstract

Emergent vegetation has a significant impact on dispersion of floating particles in open channel flow. In this thesis, we study the transport, diffusion and retention of floating particles by capillarity within emergent vegetation through an analytical model, laboratory experiments, and a numerical analysis.

We first develop a one-dimensional advection-diffusion model to analytically simulate particle transport processes within vegetated areas, and to explore the impacts of vegetation on particle transport, diffusion and removal. The random walk model of a Lagrangian approach has proven more than suitable to describe the rather unpredictable moving trajectory of particles within emergent vegetation. However, compared to the large computational costs of the Lagrangian model, which also requires more input data, a simplified model based on the Eulerian approach can be far preferable and cost-effective for rapid first-order prediction of particle transport and diffusion within vegetated areas.

Three key parameters of the standard Eulerian model of advection and diffusion with a first order decay process, namely, the mean transport velocity of floating particles, the diffusion coefficient, and removal rate of particles, are estimated from the parameters of a Lagrangian model, previously proposed for the same purpose. The validity of the parameters of the Eulerian scheme is then verified through performing a large number of realizations with the Lagrangian model. The comparison between the dispersal kernel, as well as the spatio-temporal distribution of floating particles, predicted by Eulerian model and stochastic model is quite satisfactory and suggests that the proposed Eulerian approach is properly described.

The model results indicate the large impact of temporary trapping events on the advection and diffusion of floating particles, which dramatically reduce the transport velocity compared to the bulk flow velocity, and largely increase the diffusion coefficient.

As such, we then conduct laboratory experiments to provide a better under-

standing of the propagation of floating seeds and propagules through capillarity in areas of emergent vegetation, mainly focusing on the temporary trapping events. The experimental data are also used to verify our proposed Eulerian model. In the experiments, the vegetation is simulated as an array of cylinders, randomly arranged, and seeds are simulated with small wooden spheres having almost the same diameter of the cylinders.

The temporary trapping process is found to strictly depend on the stem density and the ratio between the flow velocity and the escape velocity; the latter, representing the scale-velocity of the problem, and at least as a first approximation, can account for the main particle and stem properties needed to estimate particle propagation.

Finally, we perform a numerical analysis to gain further insight into how the mean retention time of temporary trapping process varies with the stem density and flow velocity. We speculate that the oscillation frequency of flow velocity component is strictly related to the mean retention time. We decompose the signal of time-depending flow velocity near a stem into a series of frequencies by means of the Fast Fourier transform analysis. We observe two main oscillation frequencies of the velocity. The first is the frequency of vortex shedding of the cylinder, whereas the second is the frequency of the velocity component produced by the interference of the neighbour cylinders.

The numerical model results indicate that both frequencies depend on the bulk velocity and stem density; and the mean retention time of temporary trapping process is inversely proportional to the frequency of the velocity component produced by the interference of the neighbour cylinders.

CONTENTS

LIST OF FIGURES

LIST OF TABLES

Chapter 1

Introduction

1.1 Background

Wetlands, whether it be freshwater or saltwater, provide numerous valuable services, including water purification, food protection, water storage, stabilization of shorelines, and habitat provision (Mitsch et al., 2009). As the transient zones between terrestrial and aquatic systems, wetlands also mediate the exchanges of sediment, nutrients, metals, seeds, and other contaminants (Phillips, 1989; Barko et al., 1991; Orson et al., 1992; Dixon & Florian Jr, 1993; Nepf, 1999; Cunnings et al., 2016). Wetland plants, as the common and essential component of wetland ecosystems, control these exchanges both directly through production of seeds, uptake of nutrients, capture of sediments and biological transformation and indirectly through impacting hydrodynamic conditions (Kadlec, 1995; Nepf, 1999).

Nowadays, wetland plants are suffering from depletion and degradation under the influence of intensifying human activities and climate change, making the restoration and protection of plant communities become a primary issue (O'Reilly et al., 2003; Nilsson et al., 2010). Using artificial planting to restore vegetation in the watershed not only consumes a lot of manpower and material resources, but also does not necessarily satisfy the stratified and banded distribution law of the species community under natural conditions, resulting in irrational structure and disharmonious proportions of each component, and ultimately making the ecosystem difficult maintain self-sustainability (Yuhong & Xi, 2017). Seed dispersal, as the primary constraining factor impacting species richness, structure of plant communities (Chang et al., 2008), gene flow(Jordano et al., 2007), distribution of recruitment (Garcia et al., 2005), metapopulation dynamics (Spiegel & Nathan, 2007), plant migration (Ibáñez et al., 2006), and more, plays an important role in the development and restoration of plant community in wetlands (García

et al., 2009; Schupp et al., 2010). Therefore, seed dispersal deserves our further research to improve the ecological restoration of wetlands.

Generally speaking, once a seed leaves its parental plant, its movement to the germination site can be divided into two phases, i.e., primary dispersal, the movement of a seed from the parental plant to the ground by gravity, and secondary dispersal, the movement after it has fallen to the ground (Griffith & Forseth, 2002). As seeds will be affected by wind, animals or water during the secondary dispersal, the secondary dispersal can also be divided into three different types according to the dispersal vectors, i.e., dispersal by wind (anemochory), by animals (zoochory), and by water (hydrochory) (Groves et al., 2009; Griffith & Forseth, 2002). In wetlands, hydrochory was found to mainly determine the secondary dispersal as the seeds of many species of aquatic plants are buoyant (Neff & Baldwin, 2005), and long-distance seed dispersal was also occasionally reported in the literature (Cain et al., 2000; Griffith & Forseth, 2002; McDonald, 2014), indicating the disproportionate importance of hydrochory by either expanding the distributional extend of species or providing gene flow to connect distant communities and populations (Nathan, 2006; Van der Stocken, Vanschoenwinkel, et al., 2015).

Once seeds tumble from their parental plants, some of the fallen seeds that distributed far away from their parental plants can be subsequently moved to water by overland flow or wind, while some of the seeds that distributed near their parental plants will be intercepted by the plants. On one hand, the captured seeds ensure the development of local plant populations, on the other hand, the leaving seeds provide the source for long-distance dispersal. On reaching the water, buoyant seeds float on the water surface and non-buoyant ones sink. The seeds that sink may be transported in suspension or along the stream bed, behaving similar to the sediments or neutrally buoyant particles. During this process, some of the transported seeds can interact with vegetation either submerged or emergent. The seeds that float on the water surface are transported under the influence of flowing water, surface wave or wind (Nilsson et al., 1994; Chambert & James, 2009). During this process, some of the floating seeds can also interact with the emer-

gent vegetation and be trapped by them (Sousa et al., 2007; Chang et al., 2008; De Ryck et al., 2012; Van der Stocken, De Ryck, et al., 2015).

As such, the transport of seeds within vegetated areas is definitely a fundamental process for hydrochory, as vegetation is such a common and essential component of wetlands, despite the trajectory of a seed flowing and slaloming through vegetation is rather complex and unpredictable. On one hand, plants increase vertical diffusivity and thus reduce the longitudinal hydrodynamic dispersion (Nepf, Mugnier, & Zavistoski, 1997; Nepf, 1999). On the other hand, the interactions between seeds and vegetation strongly affect the fate of seeds, promoting their retention as well as the mechanical dispersion due to the different path traveled by particles through the canopy (Nepf, Mugnier, & Zavistoski, 1997; Chang et al., 2008).

The additional mechanisms acting in vegetated flows to enhance dispersion are associated with the back-flow region within the wake behind the plant stems that may temporarily detain the flowing particles and the so-called mechanical dispersion, arising due to the separated paths and different lengths traveled by the particles while slaloming through the stem array (Nepf, Mugnier, & Zavistoski, 1997; White & Nepf, 2003). It is worth noting that in the case of suspended particles transporting through submerged vegetation, the longitudinal dispersion is slightly increased compared to non-vegetated regions (Shucksmith et al., 2011), while it is largely enhanced in the case of floating particles slaloming through emergent vegetation due to the temporary trapping events through capillarity (Peruzzo et al., 2012). In this research, we focus on the transport of floating seeds through emergent vegetation and the interaction processes between floating seeds and emergent vegetation.

The main mechanisms responsible for the interactions between floating seeds and emergent vegetation are (1) inertial impaction, which occurs when a particle deviates from a streamline because of its inertia and collides with a stem (Palmer et al., 2004; Defina & Peruzzo, 2010); (2) wake trapping, which occurs when a

particle enters the unsteady recirculation zone behind the stem (White & Nepf, 2003); (3) Cheerios effect, i.e., trapping due to surface tension, in which floating particles are attracted toward stems by the rising meniscus (Vella & Mahadevan, 2005); and (4) net trapping, which occurs where leaves and/or stems overlap enough to form a netlike structure that intercepts the floating particle (Defina & Peruzzo, 2010). When the mean gap between plant elements is large compared to the particle size, and flow velocity is moderately slow, then the Cheerios effect is the main, if not the only, mechanism impacting seed propagation, capture and diffusion (Chambert & James, 2009), which is considered in this study.

The retention process of floating particles, referring to the particles being temporarily trapped or permanently captured by emergent vegetation here rather than the retention on the ground or in the gut, plays a fundamental role in the dispersion of floating particles through vegetated regions and structuring of the riparian community (Nilsson et al., 2010; Defina & Peruzzo, 2010). When a particle is temporarily trapped by the stem, it stays on place for a random time, which is also named retention time in this study. As different plant seeds have great differences in their floating ability due to their density, size, shape, seed coat and other characteristics, with floating duration varying from a few hours to months (Nilsson et al., 2010; Carthey et al., 2016), the retention time is also an important factor deserving further research, considering the limited floating time and viability of buoyant seeds (Defina & Peruzzo, 2010).

1.2 Literature review

The trajectory of a particle flowing and slaloming through emergent vegetation is rather complex and unpredictable, two types of mathematical models are adopted to describe the propagation of floating particles. One is the stochastic model, such as the random walk model proposed by Nepf, Sullivan, and Zavistoski (1997), in which the path traveled by individual particle through emergent vegetation is described as a series of random steps associated with either Brownian motion (molecular diffusion) or turbulent eddies (turbulent diffusion). The

main mechanisms leading to the collision and capture of particles are inertia impaction and wake trapping as the observed particles are rather small compared to mean gap between plants elements. Defina and Peruzzo (2010) also proposed a stochastic model to describe the propagation of floating particles within vegetated regions according to Lagrangian approach, where the Cheerios effect and net trapping were found to be the main mechanisms responsible for the trapping. The effects of vegetation on the propagation of a particle were taken into consideration by introducing a set of probabilities to assess how often the particle may interact with, and then either be permanently captured or temporarily trapped by the stems. A large number of experimental data has confirmed the reliability of this model. Defina and Peruzzo (2012) further ascertained the validity of the stochastic model by designing new experiments to study the influence of vegetation density and flow velocity on the relevant interaction mechanisms between particles and vegetation. Peruzzo et al. (2012) developed a physical model to predict the set of probabilities proposed before by Defina and Peruzzo (2010) and advanced their previous stochastic model. Campbell, Blackwell, and Woodward (2002) developed a empirical model based on a modified random walk and not the movement of a wave front, which requires a branching random walk, to simulate both local dispersal (autochory) and aided dispersal along river corridors (hydrochory), and predicted that most of seeds would be deposited close to the release point. A similar empirical approach was used by Levine (2003) to predict the distribution of herbaceous plants and their communities. Groves et al. (2009) developed a semi-empirical model based on theory used in aerial seed dispersal modelling and fluid mechanics to predict the distance downstream that seeds are transported over short time periods. These empirical models give a generalized prediction of seed dispersal, while the impacts of vegetation on the propagation of floating particles are not taken into account.

The other type is a kinematic model based on Eulerian approach, in which the transport of particles is determined based on Euler flow field obtained by hydrodynamic modeling, and its movement resembles sediment transport. They have

been widely and successfully applied to describe the transport of particles through vegetation by assuming that the particle transport is driven by the mean flow velocity. For example, Cunnings et al. (2016) developed a one-dimensional Eulerian model to simulate buoyant A.rhombifolia seed dispersal in river channels, characterized by an advection-dispersion equation which is coupled to a transient storage model using an exponential decay term. Dispersal of salt marsh plant seeds in marsh-channel system with much more complex bidirectional flow is also modeled through numerical model Delft3D (Nitto et al., 2013), or analytical model (Shi et al., 2020). An exponential decay coefficient was introduced to account for the loss of floating seeds due to retention by emergent vegetation (Shi et al., 2020), while the impacts of emergent vegetation on transport velocity of floating seeds, and the diffusion coefficient were not considered. Recently, Liu, Zeng, Katul, Huai, and Bai (2020) assessed an Eulerian model considering the slowdown events of floating particles interacting with the vegetation stems, and found the impacts of the slowdown events on mechanical dispersion; mechanical dispersion arises when fluid particles travel different paths through the array and end up separated by a distance due to the obstruction by plant stems (Nepf, Mugnier, & Zavistoski, 1997). Since short-time slowdown events can affect the mechanical dispersion, let alone the long-time retention events. But to the best of our knowledge, an advection-diffusion model that includes long-time retention mechanisms is lacking. Note that long-time retention is often the main process promoting particle dispersion at large scales.

The retention time, which can dramatically reduce the mean transport velocity of floating particles and enhance the mechanical dispersion, is also a research emphasis of seed dispersal research, considering the limited floating time and viability of buoyant seeds. MacLennan and Vincent (1982) investigated the residence time of particles in the wakes behind flat plates, where the Reynolds number was sufficiently high leading to the occurrence of vortex shedding. Their system was referred to closely resemble the case of wake behind a cylinder by White and Nepf (2003), since the behavior of the oscillatory wakes and the von Karman vor-

tex street behind bluff bodies is nearly universal. The residence time measured by MacLennan and Vincent (1982) followed an exponential distribution, with the rate parameter to be the mean residence time. A strong dependence of mean residence time on Reynolds number was observed by them, agreeing with the Reynolds-number-dependence of the vortex-shedding frequency. Thereby they argued that the residence time is inversely proportional to the frequency of vortex shedding f_s, which is in accordance with the findings of Defina and Peruzzo (2010) as the vortex-shedding frequency is proportional to flow velocity, and Defina and Peruzzo (2010) found that the mean retention time of long-time trapping events decreases with the increasing flow velocity. Defina and Peruzzo (2010) also observed that the particle trapping events have two different retention (short- and long-) time distributions. And they then adopted a weighed combination of two exponential distributions to predict the retention time distributions (Defina & Peruzzo, 2012). The good agreement between experimental data and model result validated the exponential distribution.

Additionally, Defina and Peruzzo (2010) found that there are a significant number of temporary trapping events when an array of vertical cylinders is used to mimic a vegetation patch, while in the experiments carried out by Peruzzo, Viero, and Defina (2016), in which only one single cylinder is used, the particle either remained in the wake permanently attached to the cylinder or flowed downstream quickly after colliding with the cylinder, thus the number of temporary trapping events was negligibly small. This means as the stem density increases, the particles initially captured by the cylinders detach from the stem after a certain time, leading to the reduction of mean retention time. But why the variation of stem density can affect the interaction processes between particles and plant is still unknown, and it deserves our further research to correctly describe the dispersal of floating seeds within emergent vegetation regions.

1.3 Objectives

Based on the literature review above, we can find that a stochastic model has been developed to describe the rather complex transport processes of floating particles through emergent vegetation by previous researchers and proven to be more than suitable. However, compared to the large computational costs of the Lagrangian model, a simplified advection-diffusion model based on the Eulerian approach can be far preferable and cost-effective for rapid fist-order prediction of particle transport and diffusion within vegetated areas. Although advection-diffusion models have been widely and successfully applied to describe the transport of floating particles through emergent vegetation, the particles were assumed to be driven by the mean flow velocity, the influence of long-time temporary trapping and permanent capture events were never considered, which can significantly influence the mean transport velocity and dispersion of particles. Therefore, in this study, we first developed a one-dimensional advection-diffusion model in Chapter 2 to simulate the particle transport processes within vegetated areas, and to explore the impacts of vegetation on the transport, diffusion and removal of floating particles.

Previous laboratory experiments found that there are a significant number of temporary trapping events when an array of vertical cylinders is used to mimic a vegetation patch, while when there is only one single cylinder, the number of temporary trapping events is negligibly small. Therefore, in the Chapter 3, we carry out laboratory experiments with an array of cylinders mimicking emergent vegetation and wooden spheres mimicking floating seeds to study the propagation of floating seeds in the emergent vegetation regions, mainly focusing on the influence of stem density on temporary trapping process.

In the Chapter 4, we use the numerical model COMSOL to predict the flow field within the emergent cylinders. We speculate that the oscillation frequency of the flow velocity is strictly related to the mean retention time of temporary trapping events estimated through experiments. By comparing the frequency with

the mean retention time, we preliminarily understand the mechanism of floating particle retention time and explore the effects of flow velocity and stem density on the frequency and hence mean retention time.

Chapter 2

An Eulerian model for the transport and diffusion of floating particles within regions of emergent vegetation

To date, the Lagrangian stochastic approach has proven more than suitable to describe the propagation of particles and their interactions with the vegetation. However, the Lagrangian stochastic model is extremely demanding, both on input data and computational costs at large scales. To overcome this drawback, whenever possible, upscaling from the local interaction processes between particles and stems is desirable, and this means moving from the Lagrangian to the Eulerian approach. A simplified model based on the Eulerian approach can be far preferable and cost-effective for rapid first-order prediction of particle transport and diffusion within vegetated areas.

Advection-diffusion models have been widely and successfully applied to describe the transport of particles through vegetation by assuming that the particle transport is driven by the mean flow velocity (Richards et al., 1995; Nepf, Mugnier, & Zavistoski, 1997; Nitto et al., 2013; Cunnings et al., 2016; Shi et al., 2020). Recently, Liu et al. (2020) assessed an Eulerian model including the mechanical dispersion due to the slowdown of particles interacting with the vegetation stems, but to the best of our knowledge, an advection-diffusion model that includes long-time retention mechanisms is lacking. Note that long-time retention is often the main process promoting particle dispersion at large scales.

This Chapter aims at covering this gap in knowledge by presenting an advection-diffusion model, whose parameters are strictly related to those of the Lagrangian stochastic model proposed by Defina and Peruzzo (2010), which also accounts for long-time retention processes and particle removal by vegetation.

2.1 Methods

Since we want to develop an Eulerian model whose parameters are strictly related to those of the Lagrangian stochastic model, a short description of the latter model is given below. It is also worth pointing out that the stochastic model, originally developed to describe the transport and diffusion of floating particles, can be applied also to the case of moderately heavier than water or neutrally buoyant particles.

2.1.1 The stochastic model

The stochastic model, proposed by Defina and Peruzzo (2010), considers the generic trajectory traveled by a particle with velocity U within a region of emergent vegetation; the trajectory is dissected into segments or sections with length $\Delta s = 1/\sqrt{n}$, n being the stem density. Within each section, the particle has the probability P_i of interacting with a stem, and probability $1 - P_i$ of flowing downstream undisturbed.

When a particle collides with a stem, it can be slowed down, with probability P_s; temporarily trapped, with probability P_t; or permanently captured, with probability P_c. When a particle is temporarily trapped, it stays on place for a random time. Based on the experimental results of Defina and Peruzzo (2012), we can assume, as a good approximation, this random time is exponentially distributed with a mean value, T. Details on the mechanisms that cause temporary or permanent captures can be found in Defina and Peruzzo (2010, 2012). The layout of the model is shown in Figure 2.1.

The typical time delay in the particle propagation produced by slow-down events is of order one second, which is much shorter than temporary trapping events (Defina & Peruzzo, 2010; Liu et al., 2020). Accordingly, and for the sake of simplicity, slow-down events are neglected in this work, i.e., when a slow-down event is predicted to occur, with probability $P_s = 1 - P_t - P_c$, we assume that the particle behaves as if it did not interact with the stem at all.

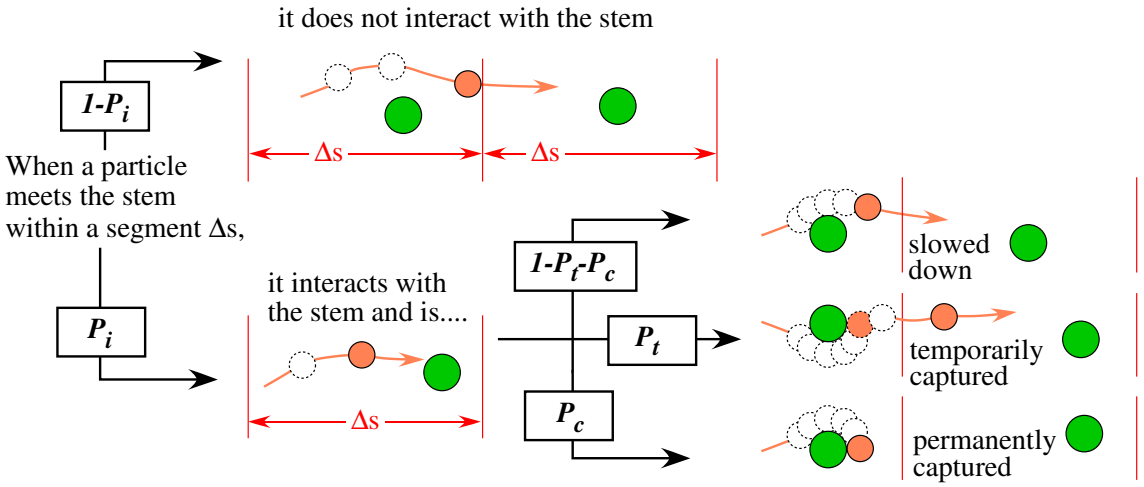

Figure 2.1 Layout of the stochastic model, adapted from Defina and Peruzzo (2010).

2.1.2 The Eulerian model

Modeling the large-scale dispersal of particles within regions of emergent vegetation with the Lagrangian stochastic model is extremely burdensome, and a model based on the Eulerian approach is far preferable. The problem then consists of relating the parameters of the stochastic model, namely, P_i, P_c, P_t, T, U, and n or Δs, to the parameters of a standard transport and diffusion model, including a first-order decay

$$\frac{\partial c}{\partial t} + U_m \frac{\partial c}{\partial x} - D \frac{\partial^2 c}{\partial x^2} = -\varphi c, \tag{2.1}$$

where c and U_m are the particle concentration and the mean transport velocity, respectively, D is the longitudinal diffusion coefficient; and φ is the capture rate coefficient that controls the fraction of particles that are permanently captured by vegetation per unit time.

The propagation of the particles described by equation (2.1) is 1D with the x-direction corresponding to the local streamwise direction, which is also the direction of the principal axis of inertia. Accordingly, the 1D model can easily be

extended to the 2D case once specified the diffusion in the transverse direction (e.g., as found by Nepf, Sullivan, and Zavistoski (1997)) that allows to construct the 2D diffusion tensor.

The temporal and spatial distribution of permanently captured particles can then be estimated as

$$\frac{\partial c_p}{\partial t} = \varphi c, \tag{2.2}$$

with c_p the concentration of permanently captured particles.

As stated above, the three parameters introduced in equation (2.1), namely, U_m, D and φ, need to be assessed by relating them to the parameters governing the stochastic model. For this purpose, the results of the stochastic model are compared with the analytical solution of equation (2.1). In particular, the propagation of a cloud of particles, of unit mass, released in $x = 0$ at $t = 0$ is simulated with the stochastic model. The solution to equation (2.1), by prescribing $c(\pm\infty, t) = 0$ as boundary condition, and $c(x, 0) = \delta(x)$, with $\delta(x)$ the Dirac delta function, as initial condition, reads

$$c(x,t) = \frac{1}{\sqrt{4\pi D t}} \exp[-\frac{(x - U_m t)^2}{4Dt} - \varphi t]. \tag{2.3}$$

The detailed derivation of the particle concentration solution is given in Appendix A. It is worth noting that, since the mass is unitary, at each instant t the concentration $c(x, t)$ represents the probability density function of the particle position.

The transport velocity U_m. Along a generic trajectory of length L through the stem array, a particle is assumed to step through $m_0 = L/\Delta s$ sections, each containing one stem; at each step, the probability that a particle collides with the stem and remains temporarily trapped is $P_i P_t$. Let T be the mean retention time, i.e., the mean time a particle remains attached to a stem at each temporary trapping event. Then the mean time, Δt, taken by a particle to traverse the length

Δs is given by the sum of the travel time, $\Delta s/U$, and the retention time, $P_i P_t T$ weighted by the fraction $(1 - P_i P_c)$ of active particles, i.e. particles that are not removed from the flow by being permanently captured by vegetation

$$\Delta t = \frac{\Delta s}{U} + \frac{P_i P_t T}{1 - P_i P_c},$$

where U is the particle velocity while freely flowing downstream without any interaction; this velocity can be approximated with the bulk flow velocity. The above equation can be rearranged to read

$$\Delta t = \frac{\Delta s}{U}(1 + \omega), \tag{2.4}$$

with

$$\omega = \frac{P_i P_t}{1 - P_i P_c} \frac{UT}{\Delta s}.$$

The mean transport velocity U_m, i.e., the mean velocity of a particle including its temporary stops, is then given by

$$U_m = \frac{\Delta s}{\Delta t} = \frac{1}{1 + \omega} U. \tag{2.5}$$

The capture rate coefficient φ. To assess the parameter φ, we refer to the case without diffusion in the Eulerian model, and hence without temporary trapping events in the stochastic model, and consider the spatial distribution of permanently captured particles as time goes to infinite; in this case, $c_p(x, t \to \infty)$ follows an exponential law (Peruzzo et al., 2012)

$$c_p(x, t \to \infty) = \frac{1}{\lambda} e^{-x/\lambda}, \tag{2.6}$$

where

$$\lambda = -\frac{\Delta s}{\ln(1 - P_i P_c)}.$$

When $t < \infty$, the distribution is given by the previous equation truncated at the distance $x = Ut$, that is

$$c_p(x,t) = \begin{cases} \frac{1}{\lambda} e^{-x/\lambda} & x \leq Ut \\ 0 & x > Ut \end{cases}. \tag{2.7}$$

In the absence of diffusion ($D = 0$) and of temporary trapping events ($P_t = 0$) the transport velocity U_m reduces to U, as stated by equation (2.5), and equation (2.1) is rewritten as

$$\frac{\partial c}{\partial t} + U\frac{\partial c}{\partial x} = -\varphi c. \tag{2.8}$$

With the initial condition given by the Dirac delta function, $c(x,0) = \delta(x)$, and boundary condition $c(\pm\infty, t) = 0$, the solution of the above equation reads

$$c(x,t) = e^{-\varphi t}\delta(x - Ut). \tag{2.9}$$

With this distribution of particles concentration, and assuming $c_p(x,0) = 0$, equation (2.2) can be solved to give

$$c_p(x,t) = \frac{\varphi}{U} e^{-\varphi x/U} H(t - x/U), \tag{2.10}$$

where $H(x)$ is the Heaviside step function. The detailed derivation is given in Appendix B. Equivalently, equation (2.10) can be written as

$$c_p(x,t) = \begin{cases} \frac{\varphi}{U} e^{-\varphi x/U} & x \leq Ut \\ 0 & x > Ut \end{cases}. \tag{2.11}$$

From the comparison of the above Eulerian solution with the solution of the stochastic model given by equation (2.7), we have

$$\varphi = \frac{U}{\lambda} = -\frac{U}{\Delta s}\ln(1 - P_i P_c). \tag{2.12}$$

We recall that the velocity U in the above equation is actually the transport velocity U_m that reduces to U when the diffusion is negligible. Consequently, in the presence of diffusion and temporary trapping events, the capture rate coefficient is still given by equation (2.12) provided that the velocity U is replaced with U_m.

The diffusion coefficient D. The diffusion of particles transported in a turbulent flow is mainly due to the mixing mechanism promoted by turbulence. However, in vegetated flows there are additional mechanisms acting to enhance dispersion (White & Nepf, 2003; Nepf, Mugnier, & Zavistoski, 1997). One mechanism is associated with the back-flow region within the wake behind the plant stems that may temporarily detain the flowing particles; this mechanism turns out to be effective only when the particle size is much smaller than the stem diameter. A more effective mechanism, which produces the so-called mechanical or hydrodynamic dispersion, arises because of the non-uniform transport velocity within the stem array, and the different length of the paths traveled by the particles while slaloming through the stems (Nepf, Mugnier, & Zavistoski, 1997).

In the case of floating particles , the temporary trapping by capillarity or by net trapping mechanism, and the associated time delay taken by particles to propagate, largely enhances the longitudinal dispersion.

The probability that a floating particle experiences k temporary trapping events while traversing m_0 sections of length Δs, has a binomial distribution (Nepf, Mugnier, & Zavistoski, 1997)

$$P(k) = C_{m_0}^k (\frac{P_i P_t}{1 - P_i P_c})^k (1 - \frac{P_i P_t}{1 - P_i P_c})^{m_0 - k}, \tag{2.13}$$

with $C_{m_0}^k$ the binomial coefficient. The mean number of delays is $m = m_0 P_i P_t / (1 - P_i P_c)$, and the variance is

$$\sigma_{m_0}^2 = m_0 \frac{P_i P_t}{1 - P_i P_c} (1 - \frac{P_i P_t}{1 - P_i P_c}). \tag{2.14}$$

After experiencing a moderately large number of sections, the binomial distribution tends toward a normal distribution with the same mean and variance; accordingly, for the case of a cloud of particles released just upstream of the vegetated area, with zero variance, after a period of time $t = m_0 \Delta t$, the spatial variance will be

$$\sigma^2(t) = \ell^2 \sigma_{m_0}^2, \tag{2.15}$$

with ℓ a suitable longitudinal length. In addition, the variance grows linearly with time as (Fischer et al., 1979; Rutherford, 1994):

$$\sigma^2(t) = 2Dt, \tag{2.16}$$

with D the diffusion coefficient. We further assume $\ell = \ell_0 U_m T$, with ℓ_0 a calibration factor, and combine equations (2.5), (2.14), (2.15) and (2.16) to yield

$$D = \ell_0^2 \frac{1 - \frac{P_i P_t}{1 - P_i P_c}}{2} \frac{\omega}{(1 + \omega)^3} U^2 T. \tag{2.17}$$

By comparing the concentration distribution provided by the stochastic model with that provided by the Eulerian model, we find $\ell_0^2 = (2 - \frac{P_i P_t}{1 - P_i P_c}) / (1 - \frac{P_i P_t}{1 - P_i P_c})$, and hence, we obtain

$$D = [1 - \frac{P_i P_t}{2(1 - P_i P_c)}] \frac{\omega}{(1+\omega)^3} U^2 T. \tag{2.18}$$

The above diffusion coefficient can be added to those stemming from other mechanisms promoting particle dispersal, e.g., mechanical and turbulent diffusion (Nepf, Mugnier, & Zavistoski, 1997). As it will be shown in Section 2.2, the long time trapping mechanism is prevalent in most cases, so that the other mechanisms promoting diffusion can be often neglected.

Overall, the parameters of the Eulerian model are given by the following set of relationships

$$\begin{cases} U_m = \frac{U}{1+\omega} \\ \\ D = [1 - \frac{P_i P_t}{2(1-P_i P_c)}] \frac{\omega}{(1+\omega)^3} U^2 T \ . \\ \\ \varphi = -\frac{U_m}{\Delta s} \ln(1 - P_i P_c) \end{cases} \tag{2.19}$$

The reliability of the solution here proposed, i.e., equations (2.19), will be assessed in the next Section through the comparison of the predictions of the two approaches; in this regard, a simple non-dimensional analysis of the parameters of the stochastic model is useful. The stochastic model is governed by the parameters P_i, P_t, P_c, U, Δs, and T; these parameters can be grouped as $P_i P_t$, $P_i P_c$, and $UT/\Delta s$. In this way, the parameters of the Eulerian model, in non-dimensional form, i.e., U_m/U, $D/U^2 T$, and φT, as given by equations (2.19), can all be written as a function of the above three non-dimensional parameters.

2.2 Results and discussion

In this Section, the results of the application of the stochastic model are compared with the solution of the Eulerian model. In particular, the propagation of a cloud of particles released in $x = 0$ at $t = 0$ is simulated both by the stochastic

and the Eulerian model.

The diffusion process described by the Lagrangian stochastic model can be considered as Fickian once all the particles experience a sufficient number of interactions. In fact, at the very beginning of the propagation process, a fraction of the cloud of particles has never interacted with the vegetation and hence has moved downstream with velocity U; all these particles, at the generic instant, t, are accumulated at $x = Ut$ and the spatial distribution of the concentration is there truncated. We then need that this fraction of particles be extremely small and hence negligible. The fraction of particles, C, that at time t has not yet interacted with any stem is

$$C = \left(1 - P_i P_c - P_i P_t\right)^{\frac{UT}{\Delta s}\frac{t}{T}}. \tag{2.20}$$

Let C_{min} be the fraction of particles that can be assumed negligibly small; according to equation (2.20) we have

$$\frac{t}{T} > \frac{ln(C_{min})}{\frac{UT}{\Delta s} ln(1 - P_i P_c - P_i P_t)}. \tag{2.21}$$

From the analysis of the results provided by the stochastic model, $C_{min} = 10^{-4}$ is found to be an acceptable threshold. An additional and independent lower boundary for the relative time t/T stems from the requirement that the initial binomial distribution must have time to evolve and approach a Gaussian distribution; this occurs when $t/T > 10 - 20$.

If $P_c > 0$, the progressive reduction of the number of the uncaptured particles makes the statistical analysis of the results, provided by the Lagrangian stochastic model, extremely demanding, particularly in the last stage of depletion of the transport process. For this reason, it is useful to consider an upper limit for the relative time t/T. A simple estimate of the number of uncaptured particles as time progresses is given by the spatial integration of equation (2.11) that yields

$$C_p = 1 - e^{-\varphi t}. \tag{2.22}$$

Actually, equation (2.11), and hence equation (2.22), can be established when diffusion is neglected; however, the results of the present numerical analysis show that equation (2.22) provides a sufficiently accurate estimate even in the presence of diffusion. In this study, the statistical analysis is limited by relative times such that $C_p \leq C_{p\,max}$, with $C_{p\,max} \approx 95\%$. Combining equation (2.19) for φ with equation (2.22), this condition can be rewritten as

$$\frac{t}{T} \leq \frac{1 - P_i P_c + P_i P_t}{(1 - P_i P_c) ln(1 - P_i P_c)} ln(1 - C_{p\,max}). \tag{2.23}$$

It is worth stressing that constraint (2.23) does not necessarily need to be satisfied. Nevertheless, it must be said that, when the fraction of uncaptured particles is very small, e.g., smaller than 5%, the relative error might be non-negligible while the absolute error is; this is the reason we confidently limited the statistical analysis to relative times that satisfy the above constraint.

In the stochastic model, the non dimensional parameters $P_i P_t$, $P_i P_c$, and $UT/\Delta s$ are allowed to vary in the following ranges

$$0 \leq P_i P_t \leq 0.9 \quad , \quad 0 \leq P_i P_c \leq 0.1 \quad , \quad 0 \leq UT/\Delta s \leq 10^3. \tag{2.24}$$

The transport velocity U_m. Figure 2.2 compares the mean transport velocity U_m given by the equation (2.5) with the mean transport velocity U_{ms} computed with the stochastic model. After a relatively short initial time, $t/T \cong 10$, the transport velocity predicted by equation (2.5) well corresponds to the one computed with the stochastic model. On the contrary, at the very early stage of the simulations, advection is the only process affecting the fate of the particles in the Lagrangian

scheme, since only a small fraction of the particles interact with the vegetation. In this condition, i.e., when $t/T \ll 1$, the velocity of the cloud centroid is close to U and hence $U_{ms}/U_m \cong 1 + \omega$.

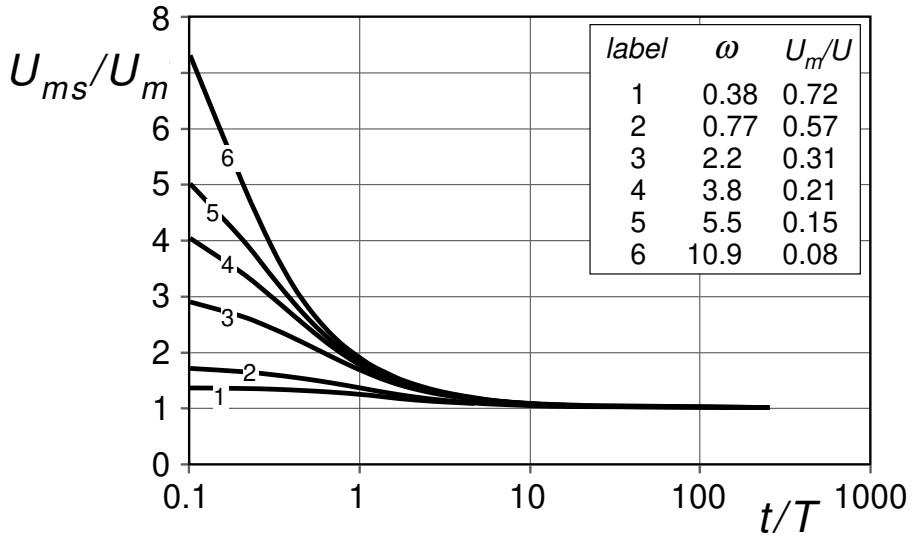

Figure 2.2 The ratio U_{ms}/U_m between the transport velocity computed with the stochastic model and that given by equation (2.5) as a function of the relative time t/T. U_{ms} has been determined by averaging over 10^5 realizations.

The capture rate coefficient φ. To check the validity of equation (2.12), predicting the parameter φ, we compare, in the absence of diffusion and temporary trapping processes, the spatial distribution of the permanently captured particles, c_p, computed with the stochastic model to that given by the Eulerian model, which is also referred to as dispersal kernel (Nathan & Muller-Landau, 2000). Figure 2.3 shows an example, among the many comparisons performed, of the fate of one cloud of 500 particles; the good agreement generally found between the analytical solution of the Eulerian model, given by equation (2.11), and the results provided by the stochastic model, confirms the correctness of equation (2.12).

In the presence of temporary trapping events, and hence of diffusion, we cannot compare the distribution $c_p(x,t)$ computed with the stochastic model with the solution of equation (2.2) since no analytical solution of this equation is available when the distribution $c(x,t)$ is that given by equation (2.3); in this case, the validity of equation (2.12) is checked by estimating with the two models the amount of

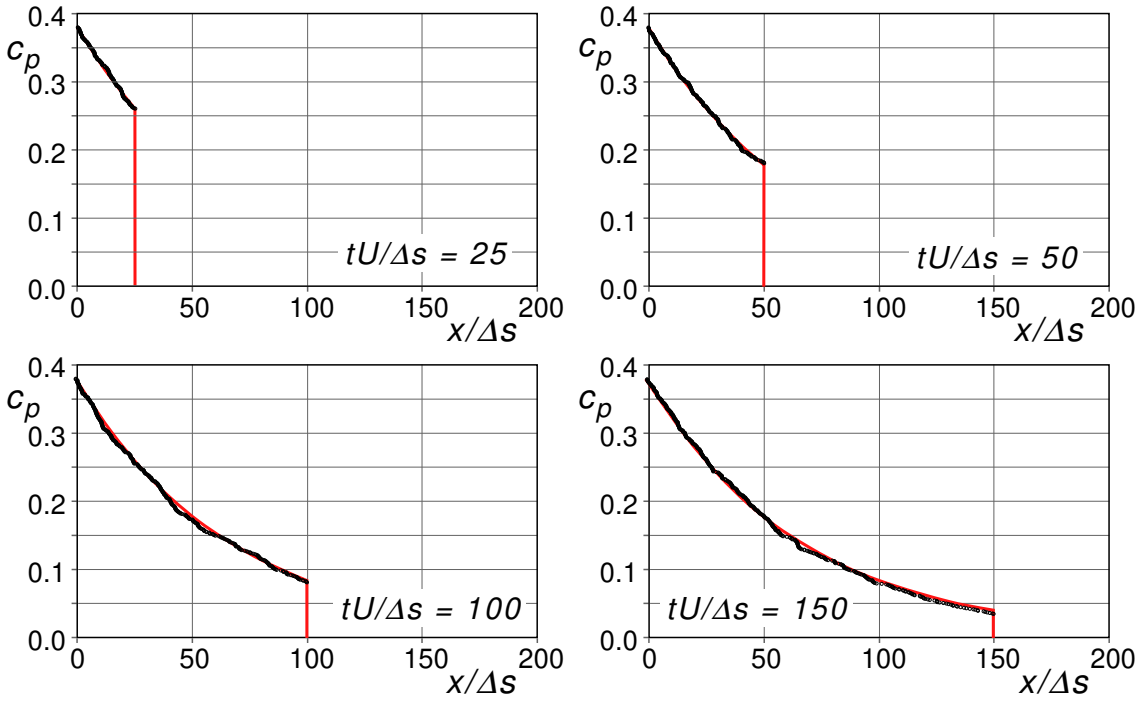

Figure 2.3 Example of the spatial distribution of captured particles concentration, c_p, at different times $tU/\Delta s$; the analytical solution of the Eulerian model, given by equation (2.11) and denoted with red lines, is compared to the results provided by the stochastic model, denoted with small black dots. In this example the parameters of the stochastic model are U = 0.05 m/s, n = 625 m^{-2} and hence Δs = 0.04 m, P_i = 0.3, P_c = 0.05, and P_t = 0. The concentration $c_p(x,t)$ computed with the Lagrangian model is estimated by releasing one cloud of 500 particles.

captured particles at different times. This procedure is illustrated later in the text.

The diffusion coefficient D. The validity of equation (2.18) relating the diffusion coefficient to the parameters of the stochastic model is preliminarily checked when the permanent capture is inhibited, i.e., $\varphi = 0$ in equation (2.1) and P_c = 0 in the stochastic model. In this case, if we release a cloud of particles with zero variance just upstream of the stem array $(x = 0)$, at $t = 0$, the variance, σ^2, of the cloud grows linearly in time according to equation (2.16).

Let ξ be the relative diffusion coefficient, $\xi = D/(U^2T)$; according to equation (2.18) we have

$$\xi = \left[1 - \frac{P_i P_t}{2(1 - P_i P_c)}\right] \frac{\omega}{(1+\omega)^3}, \tag{2.25}$$

and equation (2.16) can be rewritten as

$$\frac{\sigma}{UT} = \sqrt{2\xi}\sqrt{\frac{t}{T}}. \tag{2.26}$$

Figure 2.4 shows some examples of the non-dimensional variance $\sigma^2/(UT)^2$ as it varies with the relative time t/T for some values of the coefficient ξ; the results of the stochastic model, denoted with different symbols, strictly overlap the continuous curves given by equation (2.26), with minor differences when $t/T < 5$.

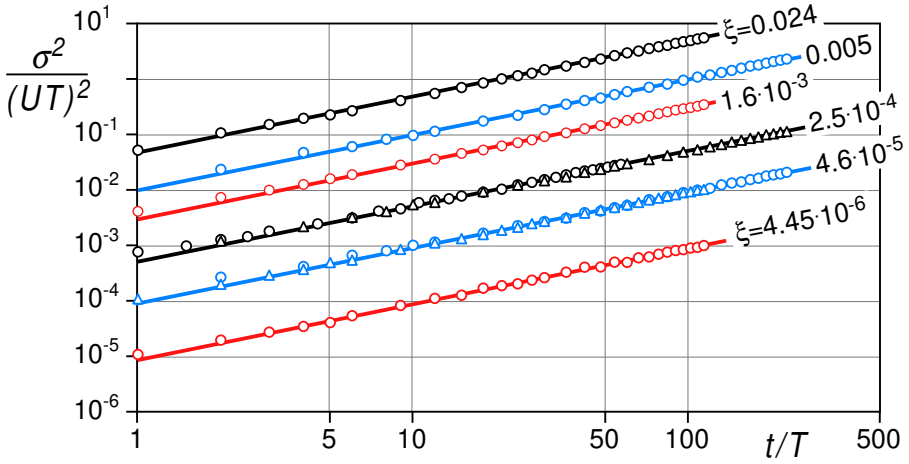

Figure 2.4 Comparison between diffusion predicted by the stochastic model and that computed with the Eulerian approach by demonstrating the non-dimensional variance $\sigma^2/(UT)^2$ varies with time t/T for some values of the coefficient ξ. In the Lagrangian model, the variance has been determined by averaging over 10^4 realizations.

The ability of equation (2.18) to predict the diffusion coefficient is also checked by comparing the results provided by the stochastic model with the solution given by equation (2.3) under different conditions.

The concentration distribution. An example of the comparison between the particle concentration distributions computed with the Lagrangian and the Eulerian models at different relative times, t/T, when the capture process is inhibited ($P_c = 0$) is shown in Figure 2.5 . The Gaussian solution satisfactorily predicts the particle distribution, despite the slight positive asymmetry that does not allow the model to perfectly capture the tails of the concentration. The fit between the computed and predicted concentration improves with increasing t/T, as the equilibrium condition between longitudinal advection and retention is approached. It is worth noting, in Figure 2.5b, that when $t/T = 5$ the distribution $c(x,t)$ is truncated at $x = 5\,UT$; this is consistent with equation (2.20) that gives $C = 8.6{\cdot}10^{-3} \gg C_{min} = 10^{-4}$. With the data of this example, the concentration is approximately distributed as a Gaussian when $t/T > 9.7$ as given by equation (2.21).

As an example, Figure 2.6 compares the particle concentration distributions computed with the Lagrangian and the Eulerian models at different relative times, t/T, when the permanent capture process is allowed. Although the probability P_c is relatively small ($P_c = 2\%$ in panel a) and $P_c = 5\%$ in panel b)), the number of flowing particles reduces quite rapidly. Importantly, we observe that the cloud centroid is slightly slower than that computed when $P_c = 0$; however, also in this more complex scenario, the Eulerian solution describes satisfactorily the time evolution of the particle concentration. In this example, as well, when $P_c = 5\%$ (Figure 2.6b), the spatial distribution of the uncaptured particles at $t/T = 5$ is truncated at $x = 5\,UT$ for the same reason discussed above.

The many simulations and comparisons performed allow us to conclude that when $t/T > 10$ and $P_c = 0$ the transport velocity and the diffusion coefficient provided by the stochastic model are ultimately time-independent. For this reason, the values of these parameters computed with the stochastic model when $t/T > 10$ can confidently be compared with the corresponding theoretical values.

Figure 2.7 compares the relative transport velocity U_m/U and the non dimen-

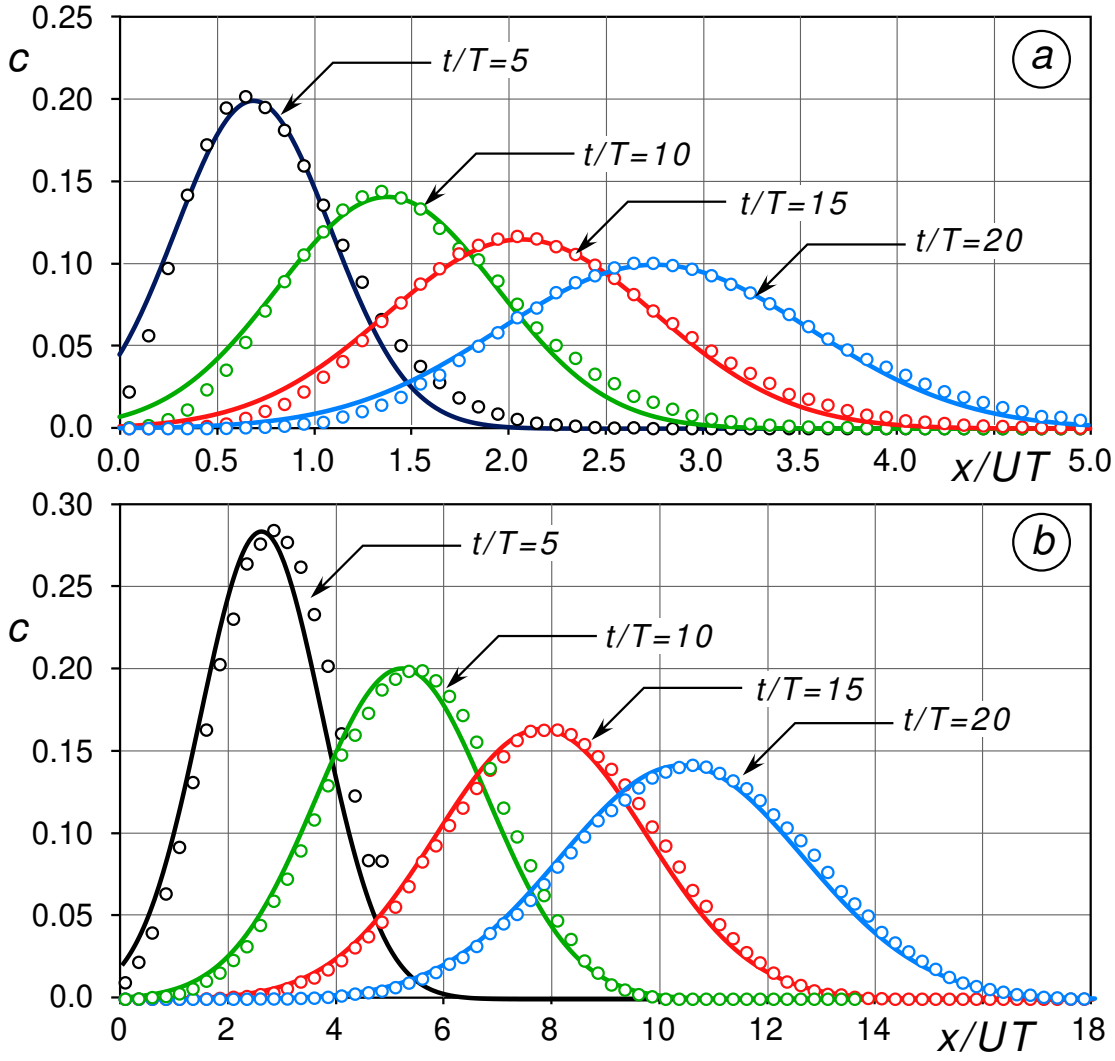

Figure 2.5 The spatial distribution of particle concentration at different times t/T; the analytical solution of the Eulerian model, denoted with thick lines, is compared to the results provided by the stochastic model, denoted with circles. In these examples the permanent capture is inhibited by assuming $P_c = 0$; the other parameters of the stochastic model are U = 0.05 m/s, n = 625 m^{-2} and hence Δs = 0.04 m, P_i = 0.1, $a)$ P_t = 0.5, T = 100 s, and $b)$ P_t = 0.3, and T = 25 s. The concentration $c(x,t)$ computed with the Lagrangian model is averaged over 10^5 runs.

sional diffusion coefficient D/U^2T computed with equations (2.5) and (2.18), respectively, with the corresponding parameters, denoted with U_{ms}/U and D_s/U^2T, evaluated with the stochastic model at $t/T = 20$ when the permanent capture is

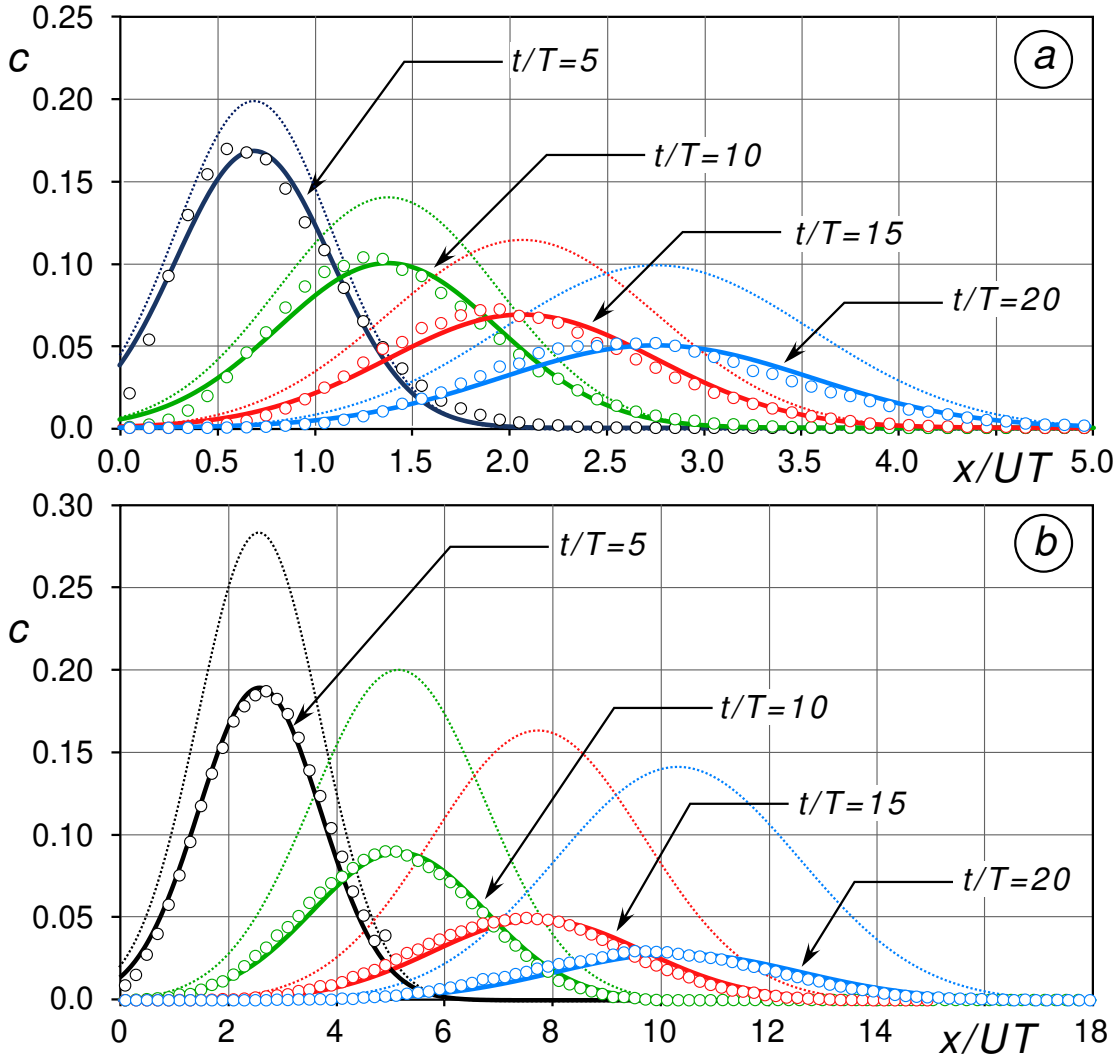

Figure 2.6 The spatial distribution of particle concentration at different times t/T; the analytical solution of the Eulerian model, denoted with thick lines, is compared to the results provided by the stochastic model, denoted with circles. In both these examples U = 0.05 m/s, n = 625 m^{-2} and hence Δs = 0.04 m, P_i = 0.1, whereas P_t = 0.5, P_c = 0.02, and T = 100 s are assumed for the case a); P_t = 0.3, P_c = 0.05, and T = 25 s, are assumed for the case b). Thin dotted lines are used to show the spatial distribution of particle concentration when P_c is set to zero. The concentration $c(x,t)$ computed with the Lagrangian model is averaged over 10^5 runs.

inhibited: the agreement is very good.

It is worth noting that, regardless the presence of the permanent capture pro-

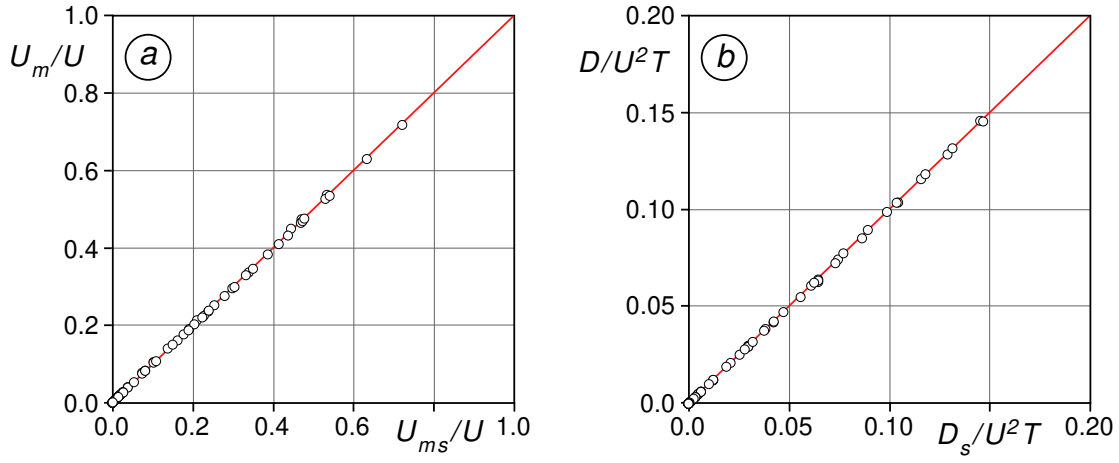

Figure 2.7 Comparison between the relative transport velocity U_m/U (panel a) and the non dimensional diffusion coefficient D/U^2T (panel b) computed with equations (2.5) and (2.18), respectively, with the corresponding parameters, denoted with U_{ms}/U and D_s/U^2T, evaluated with the stochastic model at $t/T = 20$ when $P_c = 0$. In both plots, the coefficient of determination, R^2, is larger than 0.99.

cess, the interaction between particles and vegetation, and in particular, slow-down and temporary capture processes, promotes the reduction of the particles average velocity, i.e. the transport velocity, that can be one order of magnitude smaller than the mean flow velocity. This important effect of the particle-vegetation interaction is often neglected in the standard advection-diffusive models, in which $U_m \approx U$ is assumed.

In the contemporary presence of temporary and permanent capture events things become complicated. A first important consequence is that the parameters of the Eulerian model become time dependent. Figure 2.8 shows an example of how the transport velocity U_m varies with time, from $t/T \approx 10$ to the upper boundary, given by equation (2.23), and corresponding to when 95 % of particles are permanently captured. Accordingly, the transport and diffusion process described by the Lagrangian stochastic model could not be transposed into an equivalent standard Eulerian model.

To make this point more clear, let us consider the case when permanent capture

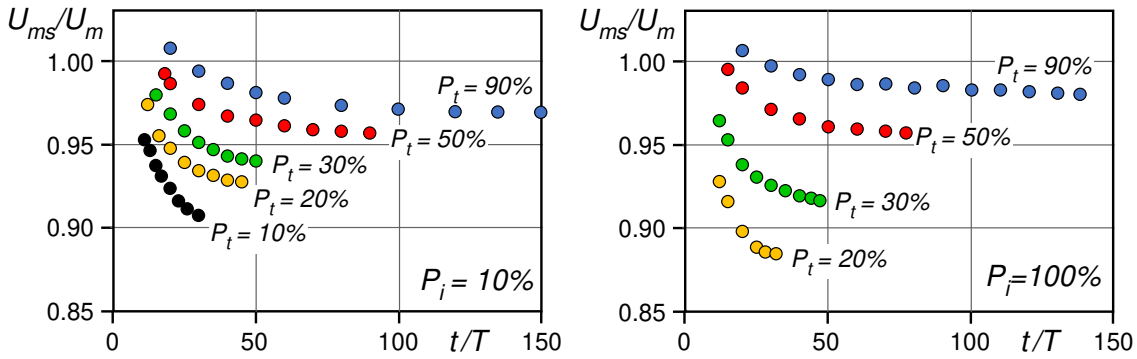

Figure 2.8 The ratio between the transport velocity computed with the stochastic model, U_{ms}, and the one given by equation (2.5), as a funtion of the relative time, t/T; in both panels $P_c = 2\%$ and $UT/\Delta s = 100$. Relative time varies from $t/T \approx 10$ to the upper boundary, given by equation (2.23).

is inhibited. After some initial time, an equilibrium condition is reached so that the rate at which particles become temporarily trapped equals the rate at which temporarily trapped particles become free again and flow downstream with velocity U. On the contrary, when both temporary and permanent capture events affect the particle flow, the above equilibrium condition cannot be achieved. This is because the number of uncaptured particles reduces in time so that the number of particles that become temporarily trapped at time t is smaller than the number of particles, previously trapped, that become free again at time t. This mechanism promotes the reduction of the number of particles that are temporarily trapped at time t. However, the number of uncaptured particles reduces faster so that, as time progresses, the ratio of particles that are staying temporarily trapped to those that are freely flowing increases and hence the mean velocity, i.e., the transport velocity, U_m, reduces in time. The same mechanism is responsible for the time reduction of the diffusion coefficient.

This point is rather interesting since we can state that the transport and diffusion process that includes some decay has memory of its previous conditions. Therefore, when modeling scenarios where the rate of permanent capture is relevant, an Eulerian model should strictly account for the history of particles propagation. However, the differences between the Lagrangian and the proposed Eu-

lerian solutions are moderately small, especially when compared with the uncertainties that typically affect the estimation of the transport velocity and diffusion coefficient when dealing with the flow through vegetated areas.

Figure 2.9 collects the results of more than 400 cases with P_iP_c, P_iP_t, and $UT/\Delta s$ varying in the ranges given by (2.24), and for different values of the relative time t/T. Black circles denote all cases when the relative time is in the range bounded by the lower and upper limits given by equations (2.21) and (2.23), respectively; gray circles denote cases when the upper constraint for t/T, i.e. (2.23), is violated whereas small white circles denote cases when the lower constraint (2.21) is violated.

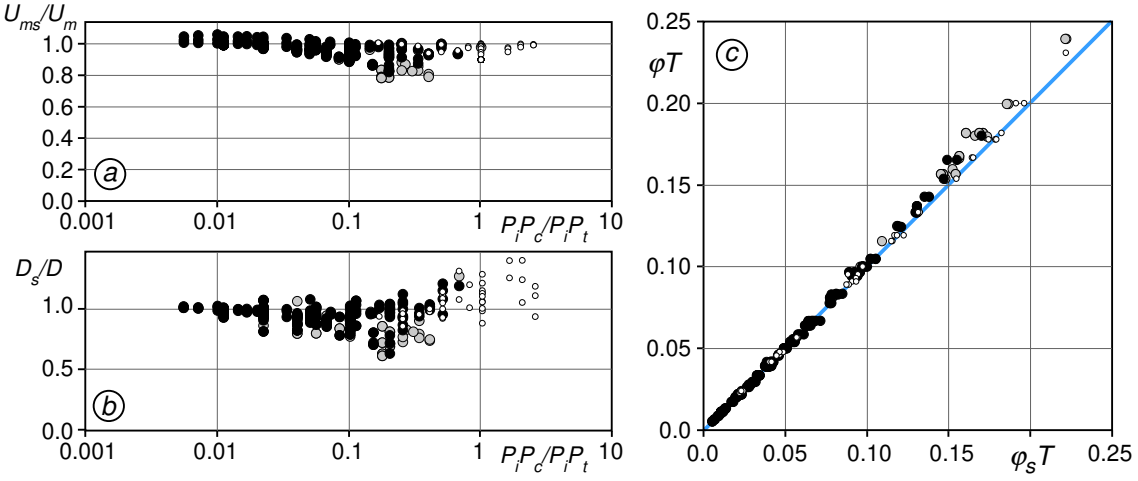

Figure 2.9 $a)$ The ratio between the transport velocity computed with the stochastic model, U_{ms}, and the one given by equation (2.5), as a funtion of P_iP_c/P_iP_t; $b)$ the ratio between the diffusion coefficient computed with the stochastic model, D_s, and the one given by equation (2.18), as a function of P_iP_c/P_iP_t; $c)$ the non-dimensional capture rate coefficient given by equation (2.19), φT, against the one computed with the stochastic model, $\varphi_s T$.

Figure 2.9a shows the ratio between the transport velocity computed with the stochastic model, U_{ms}, and the one given by equation (2.5), as a function of P_iP_c/P_iP_t. When the capture probability is relatively small, U_{ms}/U_m is close to one, while it gradually reduces with P_c/P_t increasing. When the relative time is allowed to increase beyond the upper limit given by (2.23), as expected, U_{ms}/U_m

further decreases. On the contrary, when the lower boundary for t/T given by (2.21) is violated, the ratio U_{ms}/U_m remains close to one; the reason for this behavior is that the transport velocity is nearly equal to the velocity U when t/T is small because particles experienced only a small number of long time trapping events; therefore $U_{ms} \approx U_m \approx U$.

The same reasoning explains the behavior of the diffusion coefficient shown in Figure 2.9b when the lower limit for the relative time is satisfied. When constraint (2.21) is violated, i.e., when t/T is small, the diffusion coefficient computed using the results of the Lagrangian model is larger than that predicted by equation (2.18), because the rates of temporarily retained and resumed particles are far from being in equilibrium and the spatial variance increases more than linearly with time.

The capture rate coefficient, φ, is weakly affected by the long time trapping events; Figure 2.9c confirms that equation (2.19) predicts accurately the particle removal rate when $\varphi T < 0.1$; some inaccuracies can be observed only when $\varphi T > 0.15$; however, at this removal rate, the fraction of captured particles increases very quickly. For instance, with $\varphi T = 0.15$, equation (2.22) predicts that more than 75 % of the particles initially released is permanently captured at t/T = 10, and more then 99 % is permanently captured at t/T = 30. Accordingly, the inaccuracy in estimating the rate of capture by equation (2.22) is not significant.

On the whole, given the large uncertainties that typically affect the estimation of the transport velocity and diffusion coefficient when dealing with the flow through vegetated areas, we can conclude that equations (2.19) can confidently be used to assess the parameters of a standard transport and diffusion model for particles propagating through emergent vegetation.

Comparison with available experimental results. As mentioned in Section 2.1, we use the experimental results of Defina and Peruzzo (2012) to show that, in flow regimes typically observed in natural wetlands, the transport velocity can be much smaller than the flow velocity and the diffusion coefficient can be much greater than that found for turbulent diffusion and mechanical dispersion.

Defina and Peruzzo (2012) reported a series of experiments on the propagation of floating particles through emergent vegetation. The experiments were carried out in a 6 m long flume and the model plant canopy consisted of plastic plants, randomly arranged over a 3 m long test section; plant density was n_p = 86.7 m^{-2}, and hence $\Delta s = 0.107$ m, and bulk flow velocity was in the range $U = 3.3 - 13.3$ cm/s. Wooden particles were released just upstream of the canopy and their paths through the vegetation were recorded by a camera to estimate the probabilities P_i, P_c, P_t, and the duration, T, of temporary trapping events. The results of these experiments are summarized in Table 2.1.

Table 2.1 Parameters of the Eulerian model estimated from the experimental results of Defina and Peruzzo (2012). $exp.$ denotes the same label of experiments as the one reported in Table 1 of Defina and Peruzzo (2012); U_m is the transport velocity computed with equation (2.5), D is the diffusion coefficient computed with equation (2.18), and D_t is the diffusion coefficient computed with the model proposed by Nepf (1999).

$exp.$	P_iP_c	P_iP_t	Δs (cm)	T (s)	U (cm/s)	U_m (cm/s)	D (cm^2/s)	D_t (cm^2/s)
$B1$	0.394	0.060	10.7	90	3.3	0.88	48.8	0.2
$B2$	0.287	0.065	10.7	88	5.0	1.06	74.1	0.3
$B3$	0.130	0.049	10.7	85	6.7	1.68	175.4	0.4
$B6$	0.047	0.032	10.7	80	13.3	3.06	568.2	0.8

Using equations (2.5) and (2.18), we find a transport velocity, U_m, in the range from 0.88 to 3.06 cm/s and a diffusion coefficient, D, in the range from 50 to 570 cm^2/s, respectively. It is worth noting in Table 2.1, that the transport velocity, U_m, is up to five times smaller than the flow velocity, U.

We also estimate the diffusion coefficient due to turbulence and mechanical dispersion using the model proposed by Nepf (1999); for this purpose we recall that each plastic plant used in the experiments by Defina and Peruzzo (2012) was composed of approximately 120 leaves with a diameter $d \approx 2$ mm; accordingly, the number of leaves per unit area is $n \approx 10400m^{-2}$. Using these data with equation (8) of Nepf (1999) we find the diffusion coefficients D_t listed in Table 2.1 that turns out to be dramatically smaller than those produced by the tempo-

rary trapping mechanism. The temporary trapping is hence the main mechanism promoting the longitudinal dispersion of seeds. This is further confirmed by comparing the results of the experiments performed by Defina and Peruzzo (2012) with those performed by Liu et al. (2020), in the same hydrodynamic condition, and in which the longitudinal dispersion depends on the slow-down of particles colliding with the stems. Liu et al. (2020) estimated coefficients of dispersion ranging from 2 to 4 cm^2/s, that are much smaller than those induced by long-time temporary trapping (see Table 2.1).

Interestingly, the scheme here proposed is effective also when considering slow-down processes or, equivalently, short-time trapping mechanisms. Nepf, Mugnier, and Zavistoski (1997) measured the longitudinal dispersion coefficient by releasing a conservative solute through an array of cylinders. In these experiments the mean flow velocity was $U \approx 6$ cm/s and the cylinders, with a diameter d = 6 mm, were randomly distributed with density n = 1530 m^{-2}. They also found a mean transport velocity $U_m \approx 5.5$ cm/s and a dispersion coefficient $D = 1.2 \pm 0.4$ cm^2/s. The delay of the solute particles propagation was mainly related to their trapping in the wake behind each cylinder. Accordingly, the mean retention time is likely comparable to the mean period of vortex shedding; with a cylinder Reynolds number $Re_d \approx 360$, the Strouhal number is $St \approx 0.2$ and hence $T \approx d/U\,St = 0.5$ s. On assuming that the probability that the solute particles being trapped in the wake behind a cylinder, i.e., the probability P_iP_t, is given by the fraction of volume occupied by the wakes, we have $P_iP_t \approx 0.06$. With these estimates, equations (2.5) and (2.18) give U_m = 5.6 cm/s and D = 1.0 cm^2/s, respectively. Both these values compare favorably with those found in the experiments.

Chapter 3

Retention time of floating particles captured by emergent vegetation through capillarity

Since we have known that the temporary trapping events can dramatically reduce the mean transport velocity and enhance the diffusion coefficient of floating particles, gaining further insight into the temporary trapping process is rather important. In this chapter we conduct laboratory experiments to study the propagation and retention of floating particles captured by emergent vegetation through capillarity, in particular the temporary trapping process.

Peruzzo et al. (2016) carried out experiments to estimate the probability a particle has of being captured by a stem, by releasing a large number of particles, one at a time, just upstream of one single emerging vertical cylinder. In these experiments, the particle, after colliding with the cylinder and rolling along its surface, either remained in the wake, permanently attached to the cylinder or flowed downstream; the number of temporary captures was negligibly small.

On the contrary, in the experiments in which an array of vertical cylinders is used to mimic a vegetation patch, a significant number of temporary capture events was observed (Defina & Peruzzo, 2012); in this case, the particles after hitting the cylinder and remaining stuck to it for some time, restart flowing downstream.

While we can guess the reasons for the above remarkably different behaviors, addressing and overcoming this lack of knowledge, which is one of the main objectives of the present Chapter, is crucial to correctly predict the dispersal of seeds. In fact, temporary retention is known to dramatically reduce the mean particle velocity and enhance the mechanical dispersion as is reported in Chapter 2.

3.1 Material and Methods

Before describing the experiments performed, it is worth shortly recalling the structure and the parameters of the Stochastic Lagrangian model proposed by (Defina & Peruzzo, 2010), which is described in Chapter 2 Section 2.1.1.

3.1.1 The experiments

The experiments are carried out in a 6 m long, 0.3 m wide tilting flume; water is recirculated via a constant head tank that maintains steady flow conditions. Uniform flow is achieved by adjusting the bed slope and a downstream weir; uniform flow depth is suitably chosen in the range between 10 and 15 cm in order to prevent the formation of transverse seiches induced by the vortex shedding behind the cylinders used to mimic vegetation (Defina & Pradella, 2014; Viero et al., 2017). An array of rigid wooden cylinders with a diameter d = 0.55 cm is placed on a perforated Plexiglas board to create a test section of length l = 1.43 m. In the experiments, the cylinders are emergent. Small wooden spheres of diameter d_p = 6 mm and relative density of 0.65 are released just upstream of the test section and their trajectories are recorded with two fixed mounted cameras with a frame rate of 25 s^{-1} (Figure 3.1), until the particle either flowed out of the survey area or remained trapped for more than a certain period t_{obs} (fixed equal to 600s in the present thesis). The particles are evenly painted blue to improve their observation and tracking (Figure 3.2). Recorded frames are then extracted and used to accurately determine the characteristics of each particle trajectory, i.e., the number and type of interaction events, the particle velocity, and the time that the particles spent attached to a stem when temporarily captured. The results of the experiments are summarized in Table 3.2.

We perform three series of tests (Table 3.1). In the first series, four different stem densities have been tested maintaining almost unchanged surface velocity (labels from 1 to 4). It is worth noting that when the Plexiglas board holes are fully inserted with the cylinders, the stem density is 1219, whereas the other three densities are randomly distributed. In the second series (labels from 5 to 11) and

third series (labels from 12 to 14), we keep the stem densities constant as 1219 and 610, respectively, while varying the surface velocity from 0.045 to 0.067 m/s. For each run, approximately 300 particles are individually released 1 cm below the water surface to avoid surface tension effects, at random positions in the transverse direction inside the test transect to avoid the influence of the board on the velocity.

The data of the series from $P1$ to $P4$ in Table 3.1 are the unpublished data from (Peruzzo et al., 2012). We use them to compute the mean retention time at relatively low flow velocities.

Finally, we also conduct specific experiments with one cylinder standing on the Plexiglas board, and release floating particle one by one upstream the cylinder, following the same procedure used by Peruzzo et al. (2016). For different velocities, the number of total interactions and the number of times that particle is permanently captured by the cylinder, i.e., when the particle is arrested for time larger than t_{obs}, are counted to obtain the probability of capture.

Table 3.1 Summary of experimental conditions. Experiments denoted with labels $P1$ to $P4$ are from Peruzzo et al. (2012); n is the cylinder density, U is the surface velocity.

exp.	n $(1/m^2)$	U (m/s)	Number of released particles
1	1219	0.057	293
2	914	0.057	362
3	610	0.054	317
4	243	0.055	380
5	1219	0.067	340
6	1219	0.061	357
7	1219	0.058	299
8	1219	0.045	320
9	1219	0.055	215
10	1219	0.061	166
11	1219	0.062	287
12	610	0.047	352
13	610	0.054	335
14	610	0.058	326
$P1$	1780	0.029	
$P2$	1780	0.035	
$P3$	1780	0.041	
$P4$	1780	0.047	

Figure 3.1 The experimental apparatus: side view of the test section with the array of cylinders in the most dense pattern and the two fixed mounted cameras; the flow is from left to right.

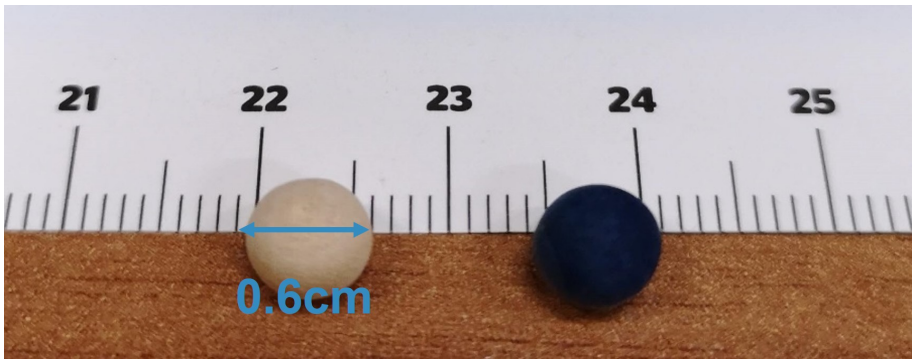

Figure 3.2 Wooden particles used in the experiments.

3.1.2 The procedure used to assess P_t and T

Since the residence time distribution does not have an upper boundary, to correctly estimate T, we should extend our observed temporary trapping events to extremely long periods. The same problem affects the estimation of the probabil-

Table 3.2 Summary of experimental data. T_{obs} is the average time spent by particles attached to a stem temporarily that lasts less than t_{obs}, N_0 is the number of segments traversed by particles, N_i is the number of particle-cylinder interactions, N_t is the number of observed long-time retention events with residence time shorter than t_{obs}, and N_c is the number of observed events with retention time $\tau > t_{obs}$ regardless of whether the particle is temporarily or permanently captured.

exp.	T_{obs} (s)	N_0	N_i	N_t	N_c
1	237	7235	2130	94	113
2	239	8171	1977	47	150
3	250	5013	1114	14	202
4	249	4234	689	8	187
5	137	15257	3282	243	49
6	139	13568	2989	237	97
7	198	7654	1757	172	161
8	249	1178	350	20	307
9	245	4930	1368	83	123
10	207	4431	1119	86	48
11	177	8268	2159	146	58
12	194	2322	453	12	331
13	250	3967	827	31	289
14	240	5256	1011	34	228
$P1$	43				
$P2$	49				
$P3$	46				
$P4$	40				

ities P_t and P_c since we need to distinguish very long-time trapping events from permanent captures. As an alternative, we can estimate T and P_t by extrapolating the results obtained from observed temporary trapping events for moderately long periods. This observation time, t_{obs}, is typically much longer than the mean retention time, T; consequently, the extrapolation is likely fairly reliable.

We consider all the temporary trapping events that last less than t_{obs}, and compute the average time spent by particles while remaining attached to a stem, T_{obs} (Table 3.2). By assuming that the residence time of temporary trapping events, τ, is randomly distributed according to an exponential probability density function

$$p(\tau) = \frac{1}{T} e^{-\tau/T}, \tag{3.1}$$

we find

$$T_{obs} = \frac{\int_0^{t_{obs}} \tau p(\tau) d\tau}{\int_0^{t_{obs}} p(\tau) d\tau} = \frac{1 - \left(1 + \frac{t_{obs}}{T}\right) e^{-t_{obs}/T}}{1 - e^{-t_{obs}/T}} T. \tag{3.2}$$

The estimated mean residence time, T, is implicitly given by equation (3.2) regardless the duration t_{obs}. The detailed processes to obtain the mean residence time T are given in Appendix C.

The estimation of the probabilities P_t and P_c is also uncertain if the observation time is relatively short. To improve the accuracy in the estimation of these probabilities, we extrapolate the observed number of captures both shorter and longer than t_{obs}, similarly to what we have done to estimate the mean residence time, T.

Let N_i be the total number of the observed particle-stem interactions, N_t the number of the observed long-time retention events with retention time shorter than t_{obs}, and N_c the number of observed events with retention time $\tau > t_{obs}$ regardless of whether the particle is temporarily or permanently captured. The ratio N_t / N_i gives the probability that a particle is temporarily trapped for a time shorter than t_{obs}. Therefore, by assuming that the distribution of residence time of temporary trapping events is given by equation (3.1), we can obtain

$$\frac{N_t}{N_i} = P_t \left(1 - e^{-t_{obs}/T}\right) ,$$

and hence

$$P_t = \frac{1}{1 - e^{-t_{obs}/T}} \frac{N_t}{N_i}. \tag{3.3}$$

In addition, the probability that a particle remains trapped for a time longer than t_{obs}, regardless of whether the capture is temporary or permanent is N_c / N_i

$$\frac{N_c}{N_i} = P_t e^{-t_{obs}/T} + P_c. \tag{3.4}$$

Once P_t is estimated with equation (3.3), P_c can be easily computed with the above equation (3.4), the detailed processes to obtain P_t and P_c are given in Appendix D.

Let X be the length of a particle traveled, during its trajectory it will meet several cylinders; we record these cylinders as potential interacting cylinders, and count the number of the potential interactions as N_0, which can be estimated as,

$$N_0 = int(1 + \frac{X}{\Delta s}).$$

As an example of the recorded particle trajectory shown in Figure 3.3, we can see the red line as a part of the trajectory of a floating particle travelling within the cylinder array. The particle potentially encounters 22 cylinders, i.e., 22 potential interacting points. The arrows indicate the actual interaction events (5), in which the particle slows down, reducing its velocity close to zero for a short time (less than 0.1 s).

The interaction probability P_i can be thus estimated by the ratio between the number of real interactions and potential interactions as below,

$$P_i = \frac{N_i}{N_0}.$$

In order to check the above assumptions and extrapolation procedures through the comparison with experimental data, we suitably combine the permanent and long-time temporary capture events, by introducing the probability that a particle remains trapped for a time τ larger than t as

$$P(\tau > t) = \frac{P_t}{P_t + P_c} e^{-t/T} + \frac{P_c}{P_t + P_c}. \tag{3.5}$$

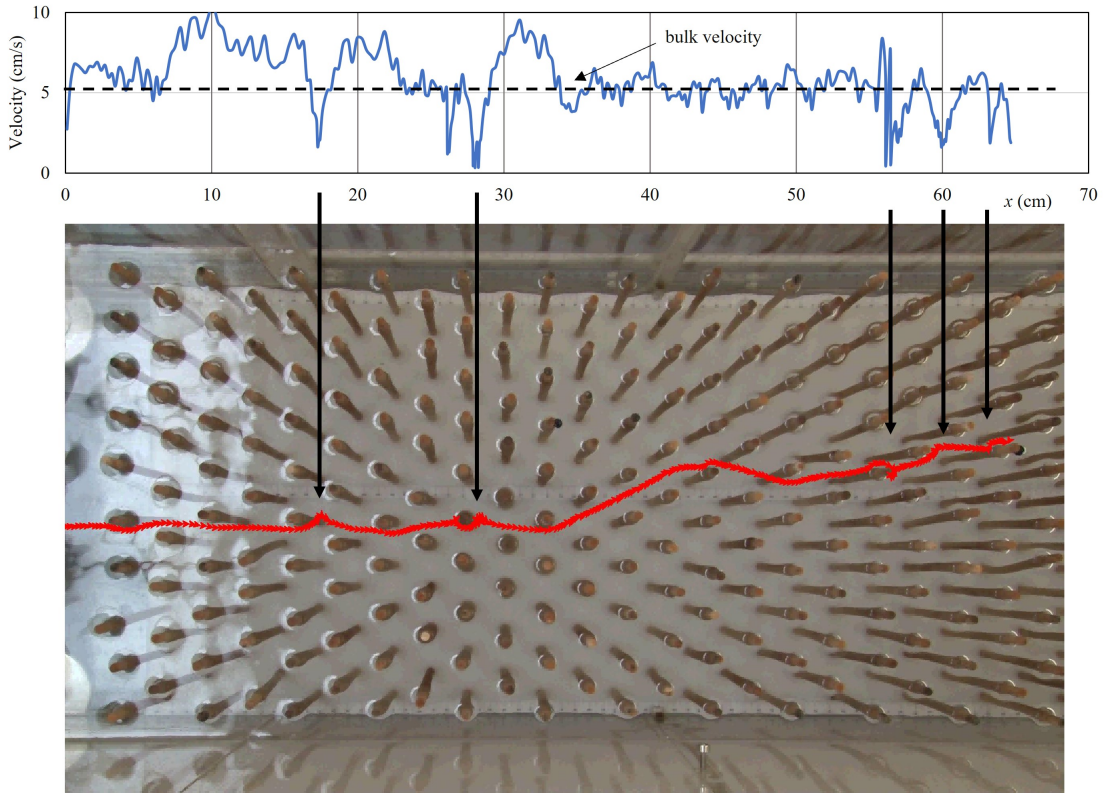

Figure 3.3 Part of the trajectory of a particle traversing the cylinder array.

3.2 Results and discussion

The assessed T, P_t and P_c. To compare the probability of exceedance given by equation (3.5) with experimental data (Table 3.3), we apply the following procedure. For each experimental condition, we sort the $N_t + N_c$ measured retention times in ascending order. The observed probability $P(\tau > t_i)$, with t_i the i-th retention time out of the $N_t + N_c$ trapping events, and $i = 1, N_t$, is then given by $P(\tau > t_i) = 1 - i/(N_t + N_c)$.

From the comparison between experimental data and equation (3.5) we observed that the mean residence time, T, estimated with equation (3.2) allows to accurately describe the rate of decay of the probability $P(\tau > t)$. On the contrary, the coefficient $P_t/(P_t + P_c)$ (and hence the coefficient $P_c/(P_t + P_c) = 1 - P_t/(P_t + P_c)$), obtained from the computed P_t and P_c with equations (3.3)

Table 3.3 Summary of present experimental results. T is the mean residence time estimated with equation (3.2); P_t and P_c are the long-time and permanent capture probabilities computed with equations (3.3) and (3.4), respectively; the last column of the table gives the value of the ratio $P_c/(P_t + P_c)$ obtained from the best fitting of experimental data to equation (3.5).

exp.	T (s)	P_t $(\%)$	P_c $(\%)$	$P_c/(P_t + P_c)$	$P_c/(P_t + P_c)$ tuned
1	461.1	6.0	3.7	0.38	0.42
2	480.9	3.3	6.6	0.67	0.69
3	583.9	1.9	17.5	0.90	0.90
4	576.3	1.7	26.5	0.94	0.94
5	147.1	7.5	1.4	0.15	0.19
6	150.1	8.1	3.1	0.28	0.30
7	273.8	11.0	7.9	0.42	0.44
8	573.4	8.6	84.7	0.91	0.92
9	534.3	9.0	6.1	0.40	0.48
10	302.2	8.9	3.1	0.26	0.30
11	218.3	7.2	2.2	0.24	0.28
12	261.7	2.8	72.8	0.96	0.97
13	594.5	5.9	32.8	0.85	0.88
14	484.4	4.7	21.2	0.82	0.82

and (3.4) respectively, needs to be slightly tuned. Figure 3.4a shows some examples of the comparison between the experimental data and equation (3.5), in which the coefficient $P_t/(P_t + P_c)$ is estimated through a best fitting procedure. Importantly, as confirmed by Figure 3.4b, the adjusted coefficient $P_c/(P_c + P_t)$ turns out to be slightly larger than the theoretical one computed with the probabilities P_t and P_c given by equations (3.3) and (3.4).

The probability of capture $P_t + P_c$, and the fraction $P_c/(P_c + P_t)$. We also observed that the fraction of captured particles that, with equal velocity U, are permanently retained, $P_c/(P_c + P_t)$, decreases with increasing stem density (see Figure 3.5). This observation is consistent with the experiments performed using one single cylinder (Peruzzo et al., 2016), in which only a negligibly small number of particles was temporarily trapped.

We speculate that the probability that a particle remains attached to a stem after colliding with it is negligibly affected by stem density n; whereas stem density controls the fraction of captured particles that are temporarily retained. Accord-

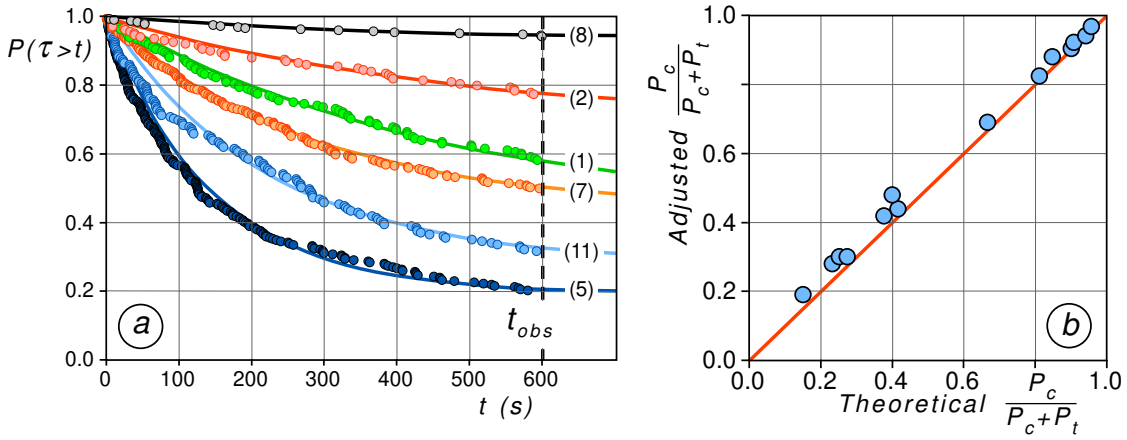

Figure 3.4 a) Comparison between experimental and theoretical residence time distribution for six different flow velocities. The circles denote the experimental data and the solid lines are given by equation (3.5); the numbers in brackets denote the experiment label. b) Comparison between adjusted and theoretical $P_c/(P_c + P_t)$.

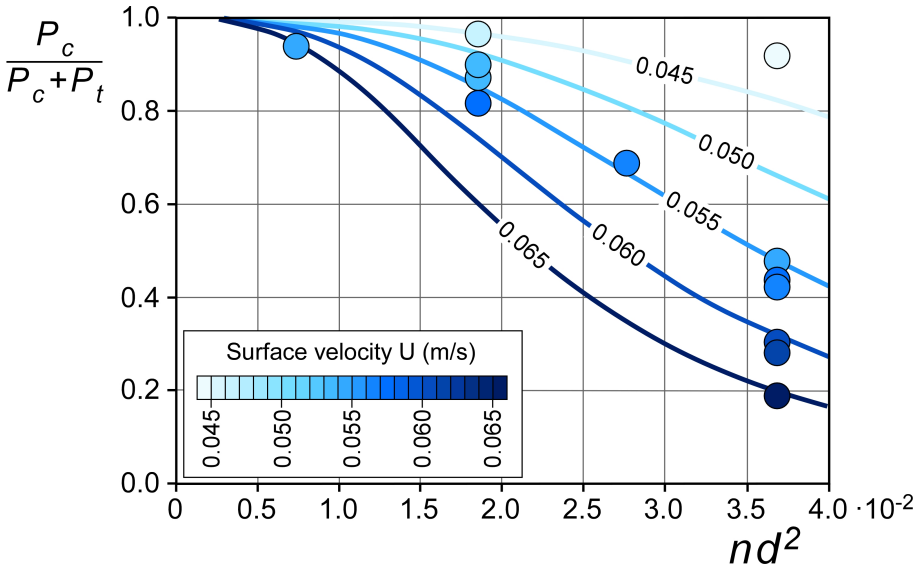

Figure 3.5 The relative probability of capture $P_c/(P_c + P_t)$ varies with the stem density, n; circles are present experimental data, the thick colored lines are from equation (3.7) for some values of the surface velocity, U.

ingly, the probability $P_t + P_c$ should not vary with stem density, and it can be predicted using the theory developed by Peruzzo et al. (2016) to estimate the capture probability, P_c, for the case of one single cylinder, when P_t was observed to be negligibly small

$$P_t + P_c = \int_0^{U_e/U} f(x)dx \qquad \text{with} \qquad f(x) = \frac{x^{\alpha-1}e^{-x/\beta}}{\beta^{\alpha}\Gamma(\alpha)}. \tag{3.6}$$

In the above equations, $f(x;\alpha,\beta)$ is the gamma distribution with $\Gamma()$ the gamma function; U_e is the escape velocity, defined to be the flow velocity such that when $U < U_e$, the probability of capture, either temporary or permanent, is greater than 95%. The latter condition relates each other the shape parameter, α, and rate parameter, β, parameters of the gamma distribution as

$$0.95 = \int_0^1 f(x)dx.$$

In order to verify this assumption, specific experiments with one single vertical cylinder are then carried out following the same procedure used by Peruzzo et al. (2016). Through a best fit between equation (3.6) and the experimental data, we find $\alpha = 90$, $\beta = 0.0094$ and $U_e \approx 0.046$ m/s. Interestingly, in these experiments the temporary trapping event is never observed.

Figure 3.6a compares the probability P_c as a function of U/U_e estimated in the experiments that use one single cylinder with the distribution of $P_c + P_t$ measured in the experiments with an array of cylinders. With some approximation, the two series of experimental data agree with each other, thus confirming the validity of the proposed hypothesis.

The reason why temporary trapping events increase with n, at the expense of permanent captures, is related to the altered hydrodynamics produced by the vegetation. In fact, vegetation enhances the turbulence and the heterogeneity of the velocity field mainly because of the vortex shedding behind each stem and their mutual interaction. Based on this reasoning, we expect that the increase of the fraction $P_t/(P_t + P_c)$ with increasing n is related to the turbulence intensity and, in particular, to the turbulent kinetic energy, k, generated by the cylinders. According to the relationship proposed by Nepf (1999) we write

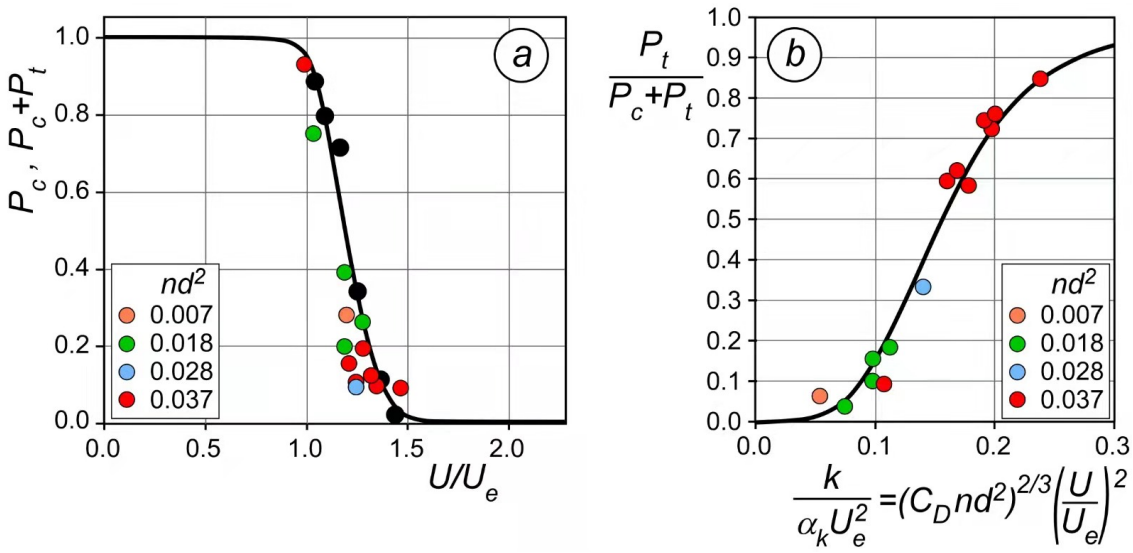

Figure 3.6 *a*) Comparison between the theoretical and experimental probability of capture as a function of U/U_e. The black circles denote the experimental values of P_c measured in the single-cylinder experiments and the black line interpolates these points according to equation (3.6); the colored circles denote the measured probability $(P_t + P_c)$ in the experiments with an array of cylinders. *b*) The fraction of particles that are temporarily captured among all the captures, $P_t/(P_t + P_c)$, as a function of the scaled turbulent kinetic energy $k/(\alpha_k U_e^2)$.

$$k = \alpha_k (C_D n d^2)^{2/3} U^2,$$

with C_D the bulk drag coefficient and α_k a calibration factor. In the present experiments, conditions are such that $C_D \approx 1$.

Figure 3.6b shows the fraction of temporary captures, $P_t/(P_t + P_c)$, as a function of the scaled turbulent kinetic energy $k/(\alpha_k U_e^2)$; the experimental data gather satisfactorily on the black solid line given by the following interpolation equation

$$\frac{P_t}{P_t + P_c} = \frac{1}{1 + \left(0.155/\frac{k}{\alpha_k U_e^2}\right)^4}. \tag{3.7}$$

The suitability of the above relationship between $P_t/(P_t + P_c)$ and $k/(\alpha_k U_e^2)$ is evident also in Figure 3.5 where equation (3.7) is plotted for some values of the

velocity U, and compared with the present experimental data.

The probability of interaction P_i. The fate of a floating particle flowing through emergent vegetation depends on the stem density, n, also because n affects the probability of interaction, P_i, i.e. the probability that the particle collides with a stem while traversing the generic segment Δs

$$P_i = \frac{b}{\Delta s} = b\sqrt{n},$$

with b the spanwise distance between the outermost trajectories, relative to the centerline, that lead a particle to collide with a stem, as is shown in Figure 3.7 (Peruzzo et al., 2012).

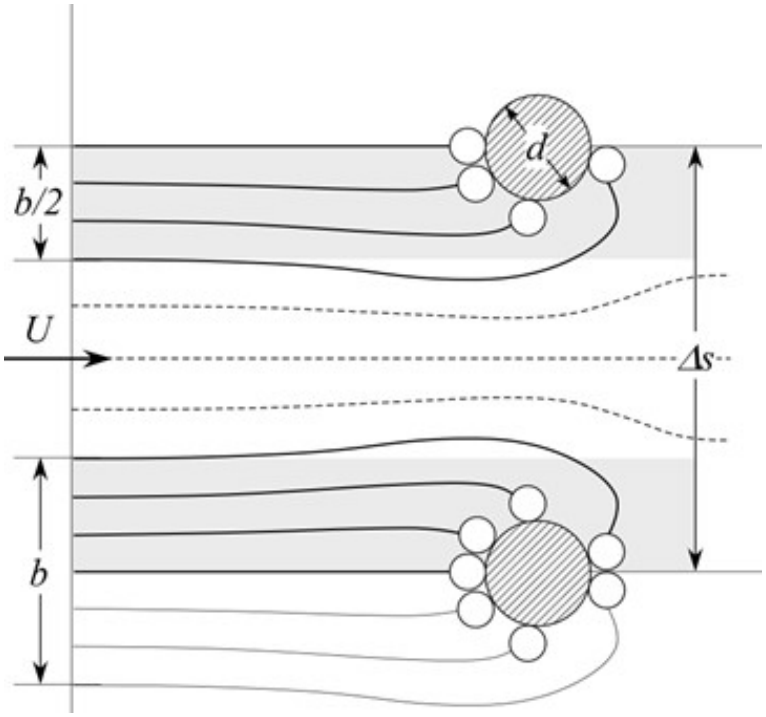

Figure 3.7 Definition sketch for the probability of a particle collision with a cylinder. Solid lines indicate particle trajectories that lead to collision, dotted lines indicate particle trajectories that will not interact with cylinder.

Peruzzo et al. (2012) provided a theoretical formulation to estimate the collector efficiency $\eta = b/d$ (Rubenstein & Koehl, 1977; Palmer et al., 2004; Peruzzo et

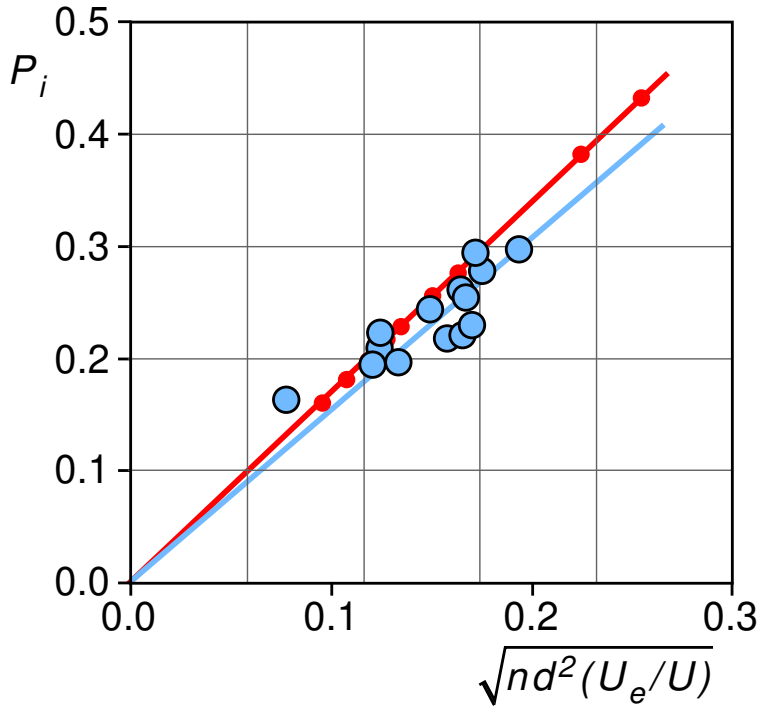

Figure 3.8 The probability of interaction P_i as a function of $[nd^2(U_e/U)]^{1/2}$. The blue circles denote present experimental data, interpolated by the blue straight line; the red line and points denote the results reported by Peruzzo et al. (2012).

al., 2013); for the given materials and size of particles and cylinders, η is inversely proportional to the square root of the ratio U/U_e. In addition, the efficiency η is linked to the probability P_i as $P_i = \eta\sqrt{n}d$ so that the probability P_i is proportional to the square root of $nd^2/(U/U_e)$. Present experimental data confirm this relationship as shown in Figure 3.8.

Figure 3.8 also shows the results reported by Peruzzo et al. (2012); the slope of the straight line that interpolates the previous data is slightly larger than that of the straight line that interpolates present experimental data. However, the slope of the interpolating line depends on the materials and size of particles and cylinders; interestingly, the fact that the two slopes are not very different from each other suggests that the influence of these characteristics are somehow well summarized by the escape velocity, U_e.

The mean retention time T. Lastly, we estimate the mean residence time, T and its dependence on the vegetation, particles and flow characteristics.

The time scale of turbulent eddies produced by the cylinders is d/U; interestingly, this time scale is also proportional to the vortex shedding period. Therefore, we use d/U to scale the mean residence time, T. We then observe that TU/d is highly and inversely related to the relative velocity U/U_e and when U/U_e is smaller than one, the probability that a particle is temporary or permanently captured when it collides with a cylinder is close to one.

When $P_t + P_c \approx 1$, residence times turn out to be extremely long and distinguishing temporary from permanent captures makes no sense; accordingly, we can confidently assume, as an approximation, that $TU/d \to \infty$ when $U/U_e \to 1$ and plot TU/d as a function of $U/U_e - 1$ (Figure 3.9).

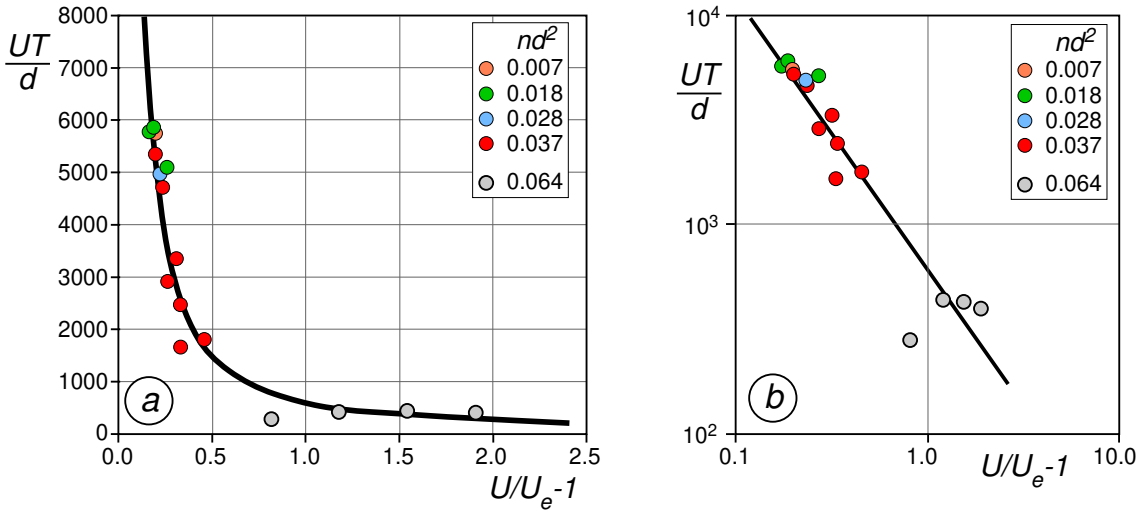

Figure 3.9 a) Mean residence time, T, normalized by the ratio d/U, as a function of $U/U_e - 1$. Gray circles denote the values estimated from the experiments performed by Peruzzo et al. (2012); the thick solid line is equation (3.8); b) same as a) in the log-log scale.

To better assess the relationship between the relative mean residence time TU/d and U/U_e, we also estimate the mean retention time, T, for some of the experiments performed by Peruzzo et al. (2012) (unpublished data). In these experiments, small wooden particles, labeled as Particle C, were continuously re-

leased upstream of an array of maple cylinders of diameter d = 6 mm and density n = 1780 m^{-2} for about 300 s. The paths of the particles, as well as their interactions with the cylinders, and retention times, were recorded with a fixed mounted camera with a frame rate of 5 s^{-1}. Four series of experiments were carried out by increasing the surface velocity, U, from approximately 2.9 to 4.7 cm/s; the escape velocity was estimated to be U_e = 1.6 cm/s, *i.e.*, appreciably smaller than that of the present experiments.

To extract reliable statistics, we reanalyze the video-recorded paths after setting the duration of the observation to t_{obs}= 150 s; we then measured T_{obs} (see Table 3.1) and estimated the mean residence time, T, with equation (3.2). The results are plotted in Figure 3.9 as the gray points.

Figure 3.9 also shows that the experimental values of TU/d as a function of U/U_e can be interpolated by the following power law

$$\frac{TU}{d} = \left(\frac{c_1}{U/U_e - 1}\right)^{c_2} \qquad \text{with} \quad c_1 = 140 \text{ and } c_2 = 1.3. \tag{3.8}$$

Interestingly, the major role that the vegetation density plays in the dynamics of floating particles by affecting the temporary retention process, and hence the mechanical diffusion, inspires some considerations about the hydrochory process in areas with emergent vegetation.

Within a newly vegetated area, with sparse vegetation, each stem can trap seeds with a large probability of permanent retention, P_c, thus promoting the local seedling establishment and vegetation thickening. With the increasing of vegetation density, flow velocity reduces, so that the interaction probability (Figure 3.8) and the probability of capture, $P_c + P_t$, (Figure 3.6a) both increases. At the same time, if the velocity reduction is not excessive, the turbulence, and hence the ratio $P_t/(P_c + P_t)$, also increases (Figure 3.6b) so that most of the captured seeds are likely retained only temporarily, thus preserving a window of opportunity for

seeds to spread longer distances and colonize new areas.

The inherent non-linearity of the particle-stem interaction process as well as the opposite effect that vegetation density and flow velocity have on the turbulent kinetic energy (Nepf, 1999), greatly add to the difficulties of predicting seeds dispersal or their definite capture and germination; thereby, the relative importance of the mechanical factors that control the evolution of a vegetation patch needs to be assessed on a case by case basis. From this mechanical point of view, the existence of a vegetation density optimal related to the vegetation type and flow regime cannot be excluded, and the issue deserves to be investigated.

The mean transport velocity U_m. We finally discuss the possibility of using equation (2.5) to estimate the mean transport velocity of floating particles, U_m. We use the experimental values for the velocity U and the interaction probability P_i, and the extrapolated values for P_c, P_t and for the mean residence time, T to compute the parameter ω, and hence the transport velocity U_m with equation (2.5).

This theoretical value for U_m is compared with the experimental one estimated with the following procedure: *1)* for each experimental condition we consider all the recorded paths, their length L_i, and the time Δt_i spent by particles to travel the distance L_i ($i = 1, N$; with N the number of paths); *2)* we then consider all the temporary trapping events lasting $\tau_{ij} < \tau_{obs}$ ($j = 1, N_j$; with N_j the number of temporary trapping events in the $i-th$ path); *3)* we compute the total time during which the particle was travelling, $T_{run} = \sum_i \Delta t_i - \sum_i \sum_j \tau_{ij}$, and the number of temporary trapping events, $N_{tt} = \sum_i L_i / \Delta s P_i P_t$; *4)* the mean transport velocity is then computed as $U_m = \sum_i L_i / (T_{run} + N_{tt} T)$.

Figure 3.10 compares the experimental mean transport velocity with the theoretical one; all points are close to the line of perfect agreement, confirming the reliability of equation (2.5).

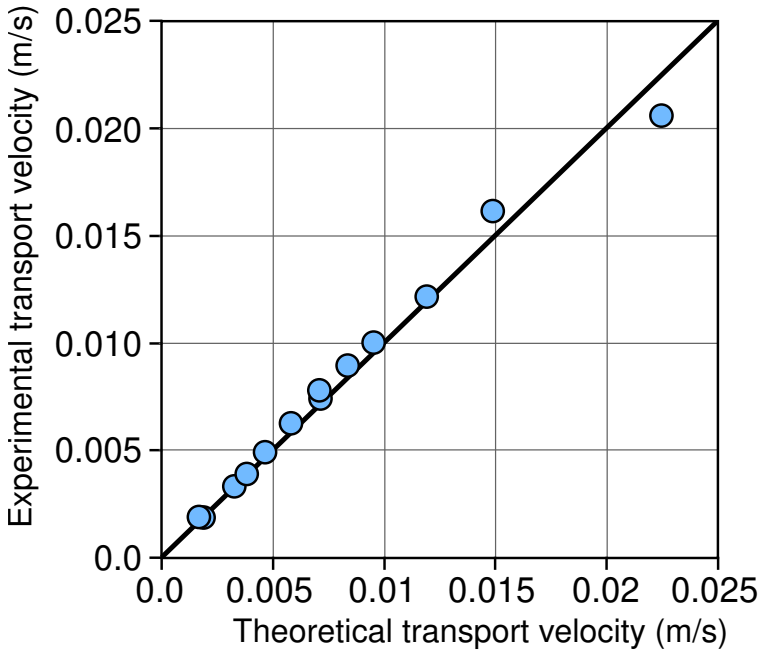

Figure 3.10 Comparison between the theoretical and experimental mean transport velocity of floating particles, U_m.

Chapter 4

Numerical analysis on the retention time of floating particles within emergent vegetation

The experimental evidences suggest that the mean retention time of temporary trapping events decreases with the increase of vegetation density and flow velocity.

For the purpose of gaining further insight into how the mean retention time varies with stem density and flow velocity, we use the numerical model COMSOL to predict the flow field within the emergent cylinders. We speculate that the oscillation frequency of flow velocity is strictly related to the mean retention time. We decompose the signal of time-depending flow velocity near a cylinder into a series of frequencies by means of the Fast Fourier transform analysis. By comparing the measured mean retention time with the corresponding oscillation frequency of flow velocity, we can preliminarily understand the mechanism of floating particle retention time and further explore the influence of stem density and flow velocity on the oscillation frequency of flow velocity around the cylinder as well as the retention time.

4.1 Numerical modelling

In this section, we use a numerical model to obtain the flow field within the stem array in the cases of different stem density and bulk flow velocity. The modeling for flow in vegetated channel was performed with an aid of commercial finite element software package COMSOL Multiphysics.

4.1.1 Governing equations

The governing equations are the continuity and Navier-Stokes equations for incompressible viscous flow:

$$\nabla \cdot \boldsymbol{u} = 0, \tag{4.1}$$

$$\frac{\partial \boldsymbol{u}}{\partial t} + (\boldsymbol{u} \cdot \nabla)\boldsymbol{u} = -\nabla p + \nu \nabla^2 \boldsymbol{u}, \tag{4.2}$$

where $\boldsymbol{u}$ is flow velocity vector, p is the pressure, and ν is the kinematic viscosity as

$$\nu = \frac{\mu}{\rho}, \tag{4.3}$$

with ρ the fluid density and μ the fluid viscosity. All simulations are carried out in COMSOL Multiphsics, which has been widely used for modeling flow around bluff bodies (Peruzzo et al., 2013; Yusuf et al., 2009).

4.1.2 Model configuration

The geometry of the model is set as two dimensional, as the variation of velocity in the vertical direction is not considered in this simulation. Accordingly, the planar velocity computed by the model neglect, as a first approximation, the effect of the air-water interface and the 3D features of the open channel flow. Due to the complexity of modeling the geometry of real natural canopies, it is common practice to approximate vegetation canopies as arrays of rigid circular cylinders (Nepf, 1999; Tanino & Nepf, 2008; Peruzzo et al., 2012; Shi et al., 2021). In this study, emergent vegetation canopies are modeled as a staggered array of cylinders with the diameter d=5.5 mm, and five rows with 20 emergent cylinders are included within the computational domain as is shown in Figure 4.1. The distance between adjacent stems is Δs, equaling to $1/\sqrt{n}$. The flow is solved in the rectangular domain, with the length $L = 5\sqrt{3}/(2\sqrt{n})$, the width $B = 4/\sqrt{n}$, n is the stem density. When flow passed through vegetation array, the vegetation forced the flow into a narrower path between vegetation stems, while the vegetation structure is assumed to be not affected, which is limited to rigid vegetation. Therefore the fluid-structure interaction physics is not considered, instead laminar

flow is used in the model.

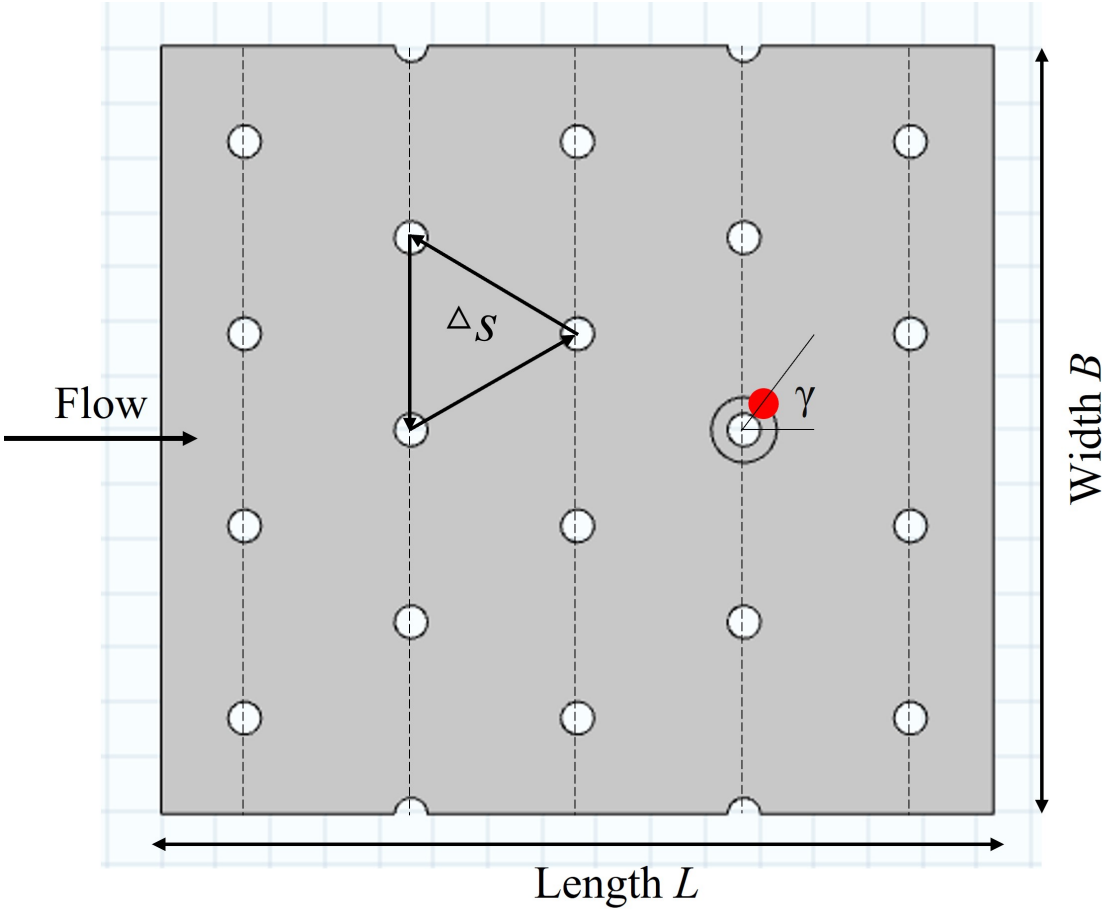

Figure 4.1 The schematic of the model geometry.

The boundary conditions are set as: *1)* no-slip no-flux boundary conditions at the cylinder surface; *2)* a fixed uniform free stream at the upstream boundary (U at x_{inlet}=0); *3)* a zero-gradient condition perpendicular to the downstream boundary at $x_{outlet} = L$; *4)* no-flux free-slip conditions at the lateral boundaries ($y = \pm B/2$). For the pressure, a zero-gradient condition is applied at all boundaries except the outlet, where a fixed value of $p_{outlet} = 0$ is set.

By using the built-in meshing function of COMSOL, the triangle mesh size of the entire region except the cylinder is set to the refinement standard of fluid dynamics.

The simulations are allowed to run for at least 2000s with a time step=0.04s to

reach a fully developed condition before any data is collected.

4.1.3 Model data analysis

We extract the flow field data at a certain circle point behind a cylinder located at the middle of the region, whose center is $(d + d_p)/2$ mm from the center of the cylinder, for example the red point shown in Figure 4.1, with an angle between the horizontal line and the line linking two circle centers as γ.

After we obtain the flow velocity over time at the red point for each run, we then use the Fourier Transform approach to decompose the flow velocity depending on time into depending on temporal frequency. We conduct the Fast Fourier Transform (FFT) through the matlab.

4.2 Results and discussion

The location for data collection. As when a floating particle is attached to the cylinder, the distance between the centers of the particle and cylinder cross-section equals to $(d + d_p)/2$, that's why we collect the data at a certain circle point behind a cylinder, whose center is $(d + d_p)/2$ from the center of the cylinder. But the value of the angle γ still needs to be investigated. We collect the flow velocity data on four different angles as $0°$, $30°$, $60°$, and $90°$, respectively, and compare the flow velocity as well as the oscillation frequency as is shown in Figure 4.2.

Interestingly, we can see from Figure 4.2a that the velocity at $\gamma = 0°$ is smallest, which is consistent with the wake zone mechanism. And the velocity increases with the increase of the angle, until $\gamma = 60°$, the mean value of the velocity at $\gamma = 60°$ (6.084 cm/s) is actually a little bit larger than that at $\gamma = 90°$ (6.043 cm/s).

Through the Fast Fourier Transform, we obtain the frequency components of the velocity as is shown in Figure 4.2b. It is worth noting that there exists two peaks, whose abscissa values represent two frequencies, the abscissa value of the star one represents the frequency of the vortex shedding, f_s, we define it as the

primary frequency, and the abscissa value of the triangular one represents the frequency of the velocity component, f_t, produced by the interference of the neighbour cylinders, we define it as secondary frequency.

Although the velocity at different collecting angle is different, the frequency keeps constant. This phenomenon is within our expectations and very reasonable. As such, we collect the data at angle $\gamma = 60^\circ$ later in this research.

The frequency of vortex shedding f_s. By setting the stem density constant and altering the bulk velocity, we obtain the data of the flow velocity over time in the case of different bulk velocities within the cylinder array. And then using the Fast Fourier Transform, we obtain the frequency components of the velocity as is shown in Figure 4.3.

We can find that the frequency of vortex shedding f_s increases with bulk velocity, which is consistent with the theory reads

$$f_s = \frac{S_r U}{d}, \tag{4.4}$$

where S_r is the Strouhal number. It is worth noting that for a single isolated cylinder, the Strouhal number S_{r0} can be obtained by the following equation (Fey et al., 1998)

$$S_{r0} = S_r^* + \frac{m}{\sqrt{R_e}}, \tag{4.5}$$

with R_e the Reynolds number ($R_e = Ud/\nu$), and different constant parameters S_r^* and m. On the contrary, for an array of cylinders, the Strouhal number increases with stem density (Ziada, 2006).

From Figure 4.4 we can find, the blue points are far from the line of perfect agreement, indicating that the frequency of vortex shedding from a single cylinder, f_{s0}, computed with S_{r0}, is smaller than f_s obtained through the numerical model, which can be attributed to the effects of stem density. The modeled frequency f_s is obtained in the case of stem density=1200 m^{-2}, while the computed frequency

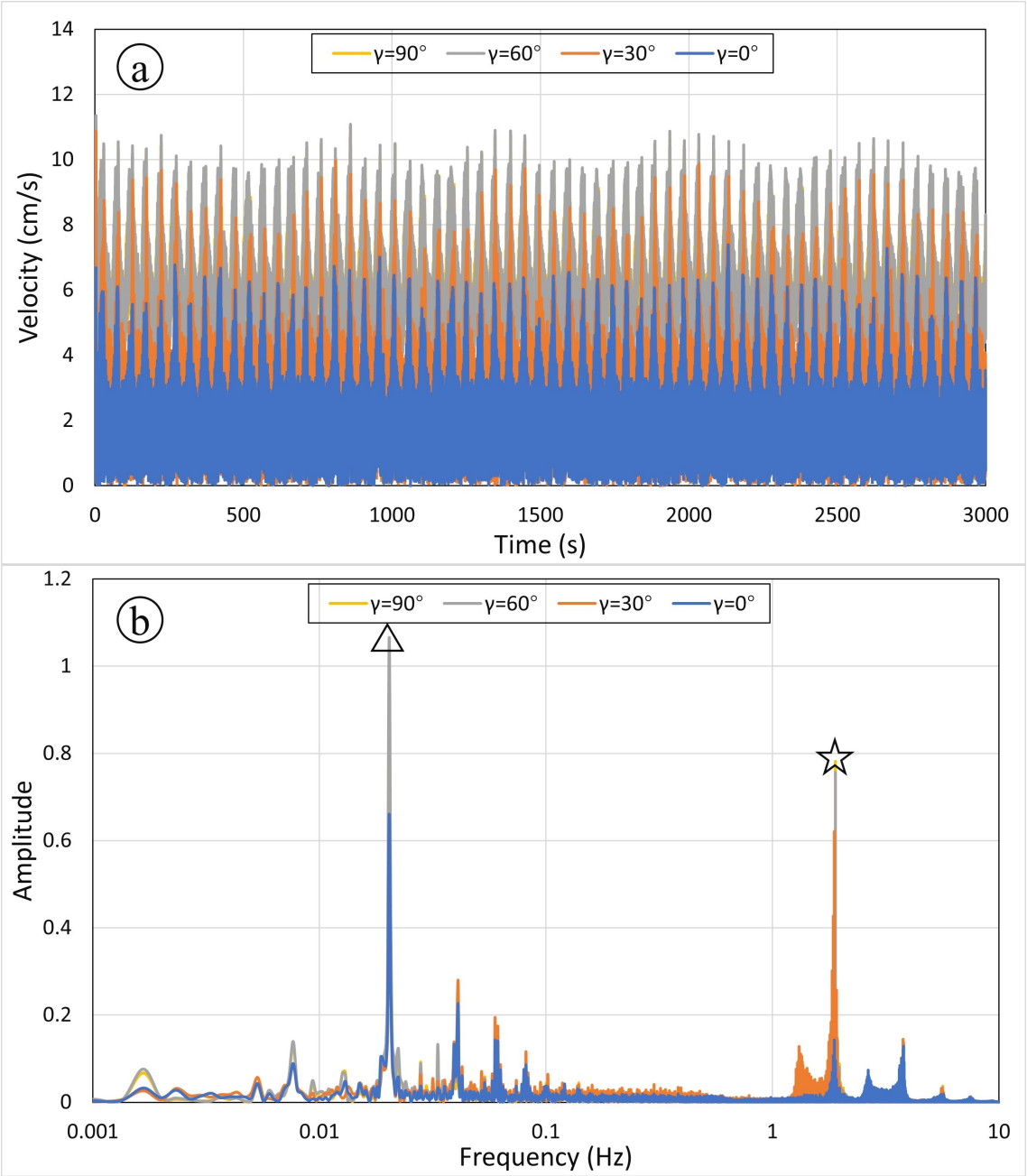

Figure 4.2 a) The velocity varies with time and b) the corresponding amplitude spectrum varies with frequency at a certain point behind the stem while different angles γ in the case of bulk velocity=5.1 cm/s, stem density=800.

f_{s0} is obtained from a single cylinder.

This behaviour indicates that vegetation density plays an important role in the hydrodynamic conditions within the vegetated regions. It largely increases the

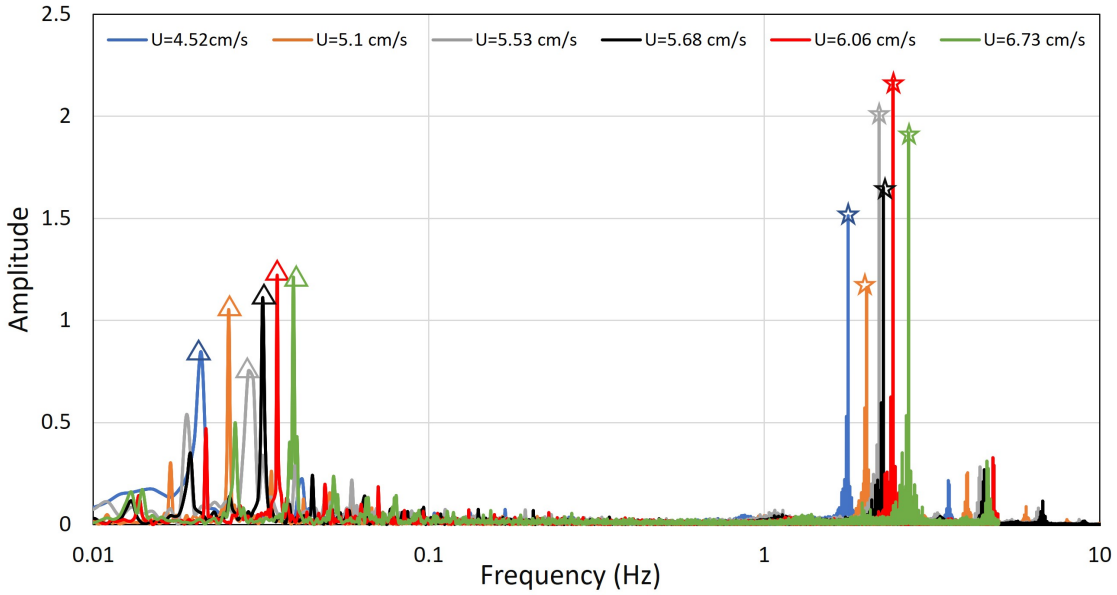

Figure 4.3 Amplitude spectrum of flow velocity in the case of stem density=1200 m^{-2}.

velocity around the cylinders and hence the frequency of vortex shedding f_s.

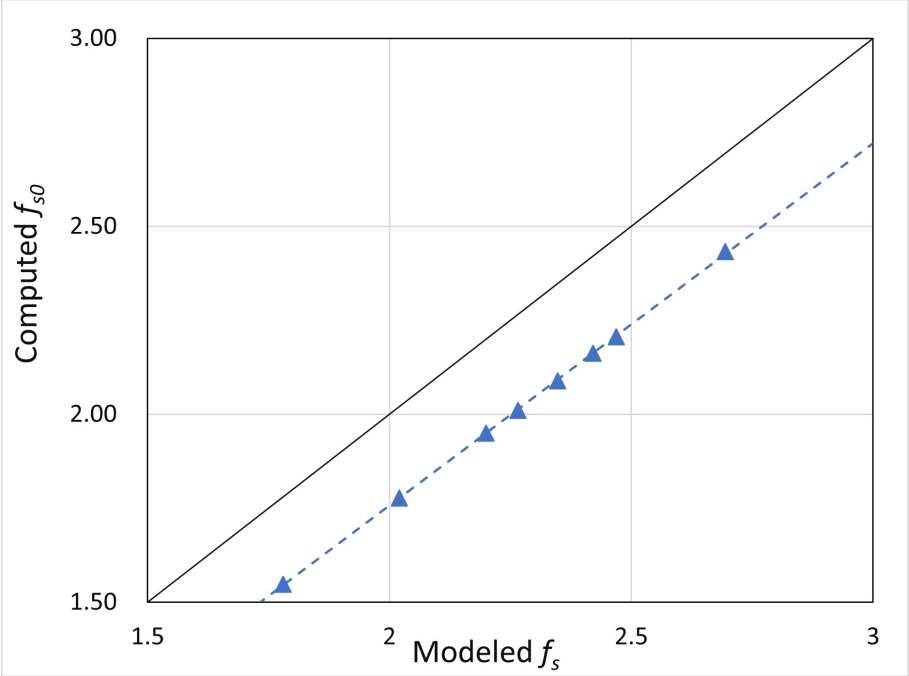

Figure 4.4 The comparison between computed frequency of vortex shedding from a single cylinder f_{s0} and modeled frequency f_s in the case of stem density=1200 m^{-2}.

It can be further confirmed by the Figure 4.5, where we plot the relative frequency of vortex shedding f_s / f_{s0} varying with stem density with constant bulk velocity. As we can see, the relative frequency f_s / f_{s0} starts from 1 and gradually increases with stem density. This result is consistent with previous findings that Strouhal number increases with stem density since Strouhal number is proportional to the vortex shedding frequency (Ziada, 2006).

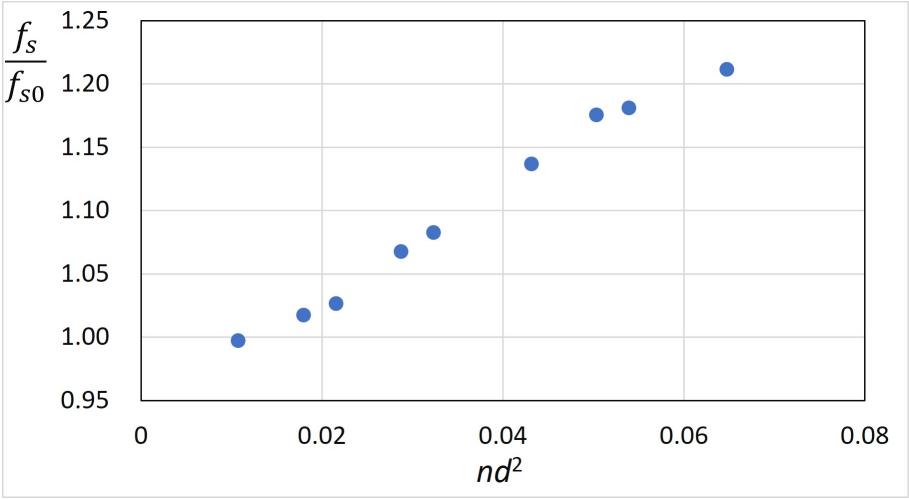

Figure 4.5 The relative frequency of vortex shedding f_s / f_{s0} varies with stem density with bulk velocity=5.1 cm/s.

The secondary frequency f_t. f_t represents the frequency of the velocity component produced by the interference of the neighbour cylinders. As is shown in Figure 4.3, the abscissa value of the peaks marked by the triangle represents the value of f_t in the cases of different bulk velocities, and the figure presents that f_t increases with the increment of the bulk velocity U, which is similar to f_s; figure 4.6a also confirms that f_t is proportional to f_s. Therefore, the oscillation period of this velocity component f_t^{-1} decreases with the increment of bulk velocity. Since we have known that the mean retention time T also decreases with the increase of flow velocity from Chapter 3, we speculate that the period f_t^{-1} is proportional to the mean retention time T.

Figure 4.6b confirms that mean retention time is proportional to the oscillation period of the velocity component produced by the interference of the neighbour

cylinders.

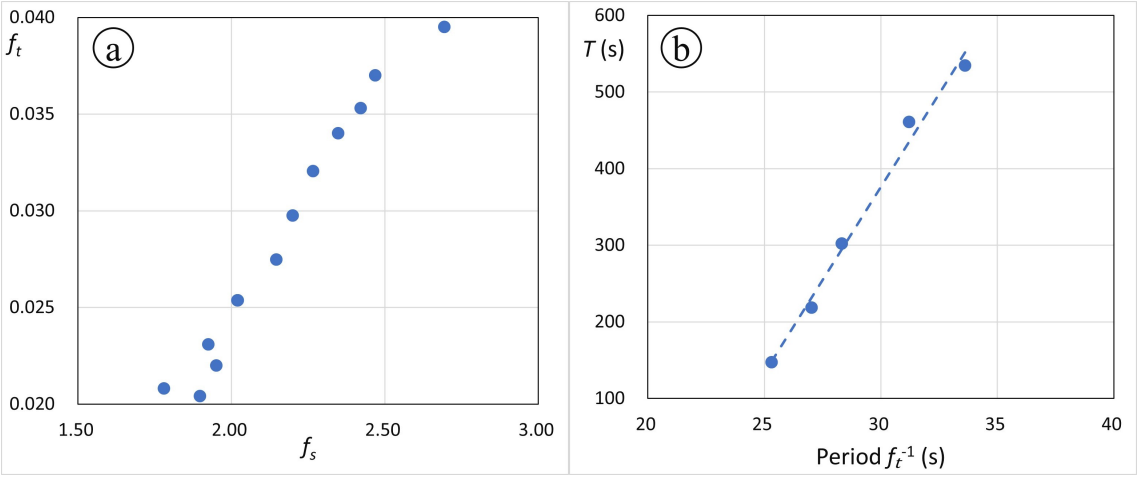

Figure 4.6 a) Comparison between frequency f_s and f_t, b) Comparison between mean retention time and the period, with stem density=1200 m^{-2}.

Since f_t is proportional to f_s, and stem density can influence the frequency f_s by affecting the velocity around the cylinders, we thus expect that the variation of stem density can also influence the frequency f_t by affecting the field field around the cylinders, and hence the period f_t^{-1}. As is shown in Figure 4.7, the period monotonically decreases with the increment of stem density in the case of constant bulk velocity, which confirms again that the period f_t^{-1} is proportional to the mean retention time T, as T also decreases with the increase of stem density according to the findings in Chapter 3. It is worth pointing out that when there is only one single cylinder, we expect that the frequency f_t produced by the interference of the neighbour cylinders would approach to zero, and hence the period f_t^{-1} would approach to infinite, corresponding to the permanent capture whose mean retention time is also infinite.

On the whole, we can conclude that when the floating particles travel within the vegetated regions, the velocity around the stems is characterized by two oscillation frequencies. The first is the primary frequency, i.e. the frequency of vortex shedding; the second is the frequency of the velocity component produced by the interference of the neighbour cylinders. Both frequencies depend on the stem density n and bulk velocity U. Interestingly, the secondary frequency seems inversely

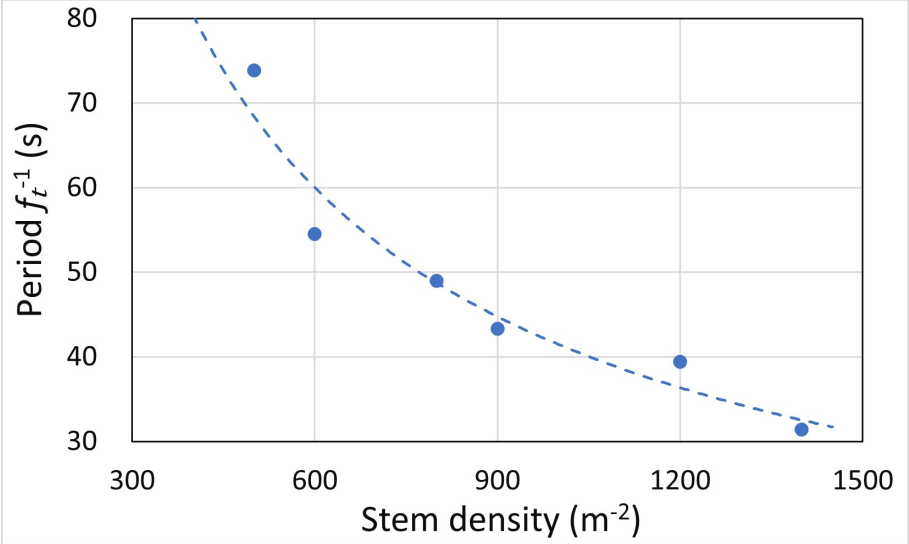

Figure 4.7 The period varies with stem density with bulk velocity=5.1 cm/s.

proportional to the mean retention time of floating particles.

Chapter 5

Conclusions

In this research, we studied the transport, diffusion and retention of floating particles within emergent vegetation.

We first presented an Eulerian model that also accounts for the particle removal due to the vegetation. The model parameters were estimated based on the parameters of the stochastic Lagrangian model proposed by Defina and Peruzzo (2010, 2012) and suitably designed for the same purpose.

The impact of the temporary trapping events on the advection and diffusion of the floating particles is very large. On one hand, the transport velocity dramatically reduces compared to the bulk flow velocity. On the other hand, the diffusion largely increases resulting in dispersion coefficients dramatically larger than those predicted by the classical mechanical dispersion theory (Nepf, Mugnier, & Zavistoski, 1997).

When the permanent capture by vegetation is inhibited, the proposed relationships between the parameters of the Lagrangian stochastic model and those of the Eulerian model are very accurate. On the contrary, in the contemporary presence of diffusion and permanent capture events, a standard advection-diffusion model could not be strictly used to describe the propagation of floating particles through emergent vegetation. In this condition, the parameters of the model become time-dependent, see, e.g., the transport velocity, U_m, in Figure 2.8. Nevertheless, the impact of time dependency is relatively small and the solution given by the proposed relationships satisfactorily predicts the Lagrangian propagation of floating particles through emergent vegetation; in most of the investigated conditions the error is smaller than 15%.

The time dependence of the parameters of the Eulerian model in the presence

of permanent capture events is an interesting and important issue. It deserves further investigation in order to model floating particle dispersion through vegetation more accurately.

Since the temporary trapping events have a large impact on the advection and diffusion of floating particles, we then conducted flume experiments to extend knowledge about the interaction processes between emergent vegetation and floating particles, such as seeds and propagules. In particular, we focused on the temporary trapping process that greatly affects the particle dispersion.

On one hand, we have verified that the probability with which a particle is captured by a stem is independent of whether the retention is temporary or permanent. In other words, the probability $P_c + P_t$ in the present experiments corresponds to the probability of permanent capture in the experiments with one single cylinder performed by Peruzzo et al. (2016), in which a negligibly small number of temporary capture events was observed.

On the other hand, we observed that the fraction of captured particles that, with equal velocity U, are temporarily retained, $P_t/(P_c + P_t)$, increases with stem density. This behavior is found to be strictly related to the turbulent kinetic energy produced by the vegetation. We also proposed a simple equation relating $P_t/(P_c + P_t)$ to k that fits well to the experimental data.

The probability $P_c + P_t$ as well as the relative mean retention time TU/d, in the temporary capture events, are both a function of the relative flow velocity U/U_e; when U/U_e is smaller than approximately one, then $P_t + P_c \cong 1$, and the relative retention time approaches to infinity.

We found that the escape velocity turns out to be a key parameter controlling the fate of floating seeds and propagules; in fact all model parameters, i.e., P_i, $P_t + P_c$, and T, scale with U_e. Together with U_e, the vegetation density, n, plays a major role in the dynamics of floating particles by affecting the interaction probability and, especially, the temporary retention process, hence the mechanical

diffusion.

Finally, the performed numerical analysis suggests a deep connection between mean retention time of temporary trapping events and flow velocity and vegetation density. We find that when the flow traverse the vegetated regions, the velocity around the stems is characterized by two oscillation frequencies. The first is the primary frequency, i.e. the frequency of vortex shedding; the second is the frequency of the velocity component produced by the interference of the neighbour cylinders. Interestingly, the secondary frequency seems inversely proportional to the mean retention time of floating particles estimated in our experiments.

In the simulations, both frequencies depend on the bulk velocity U and stem density n. When velocity increases, the two frequencies augment, and hence mean retention time of floating particles decreases due to the larger secondary frequency.

With the growth of the vegetation density, the velocity around the stems largely increases, leading to the increment of the primary and secondary frequency, and hence the decrease of the mean retention time, confirming the results of Chapter 3.

Future development could focus on the deeper exploration about the relationship between oscillation frequency and mean retention time of temporary trapping events. We have found that mean retention time T seems inversely proportional to the secondary frequency f_t, and hence proportional to the period f_t^{-1}, more experimental data would be useful to further ascertain the relationship; moreover we also noticed the different magnitudes between T and f_t^{-1}, thus what is the time scale of T is our concern and deserves further research.

In addition, from an ecological perspective, further understanding of the interaction and retention mechanisms of floating seeds with emergent vegetation would benefit the assessment of the vegetation patch evolution, the existence of a vegetation density optimal related to the vegetation type and flow regime deserves further investigation.

Notation

b	the distance between the outermost trajectories that lead to a particle colliding with a stem
B	the width of model domain
c	particle concentration
C_D	bulk drag coefficient
c_p	concentration of being permanently captured particles
D	longitudinal diffusion coefficient
D_s	longitudinal diffusion coefficient computed with stochastic model
D_t	longitudinal diffusion coefficient computed with previous model
d	diameter of cylinder
d_p	diameter of particle
f_s	frequency of vortex shedding
f_t	frequency of the velocity component produced by the interference of the neighbour cylinders
H	Heaviside step function
k	turbulent kinetic energy
l	length of the test section
L	length of model domain

m	a constant parameter to calculate the Strouhal number
m_0	the number of sections within the trajectory
n	stem density
N_0	number of segments traversed by particles
N_i	number of particle-cylinder interactions
N_t	number of observed long-time retention events shorter than t_{obs}
N_c	number of observed events with retention time longer than t_{obs}
P_i	probability that a particle interacts with a stem
P_s	probability that a particle is slowed down after interacting with a stem
P_t	probability that a particle is temporarily trapped by a stem after interacting with the stem
P_c	probability that a particle is permanently captured by a stem after interacting with the stem
p	pressure
R	retention rate
R_e	Reynolds number
S_r	Strouhal number
S_r^*	a constant parameter to calculate the Strouhal number

T	mean value of all retention times
T_{obs}	mean value of observed retention times which are shorter than t_{obs}
t_{obs}	a defined time boundary
U	particle velocity while freely flowing downstream without any interaction
U_m	mean particle velocity
U_{ms}	mean particle velocity computed with stochastic model
U_e	escape velocity, below which, the probability of capture, either temporary or permanent, is greater than 95%
$\boldsymbol{u}$	flow velocity vector
α	shape parameter of gamma distribution
α_k	calibration factor
β	rate parameter of gamma distribution
Δs	length of each section within the travelling trajectory of particles
Δt	time taken by a particle to traverse the length of Δs
δ	Dirac delta function
η	collision efficiency of the stem
Γ	the gamma function

γ	angle between the horizontal line and the line linking the center of record circle and cylinder circle
λ	particle mean path length before being permanently captured
μ	fluid viscosity
ν	kinematic viscosity
ω	dimensionless parameter
ϕ	solid volume fraction
ρ	fluid density
τ	retention time
φ	capture rate coefficient
φ_s	capture rate coefficient computed with the stochastic model

References

Barko, J. W., Gunnison, D., & Carpenter, S. R. (1991). Sediment interactions with submersed macrophyte growth and community dynamics. *Aquatic botany*, *41*(1-3), 41–65.

Cain, M. L., Milligan, B. G., & Strand, A. E. (2000). Long-distance seed dispersal in plant populations. *American journal of botany*, *87*(9), 1217–1227.

Campbell, G. S., Blackwell, P., & Woodward, F. I. (2002). Can landscape-scale characteristics be used to predict plant invasions along rivers? *Journal of Biogeography*, *29*(4), 535–543.

Carthey, A. J., Fryirs, K. A., Ralph, T. J., Bu, H., & Leishman, M. R. (2016). How seed traits predict floating times: a biophysical process model for hydrochorous seed transport behaviour in fluvial systems. *Freshwater Biology*, *61*(1), 19–31.

Chambert, S., & James, C. (2009). Sorting of seeds by hydrochory. *River Research and Applications*, *25*(1), 48–61.

Chang, E. R., Veeneklaas, R. M., Buitenwerf, R., Bakker, J. P., & Bouma, T. J. (2008). To move or not to move: determinants of seed retention in a tidal marsh. *Functional Ecology*, *22*(4), 720–727.

Cunnings, A., Johnson, E., & Martin, Y. (2016). Fluvial seed dispersal of riparian trees: transport and depositional processes. *Earth Surface Processes and Landforms*, *41*(5), 615–625.

Defina, A., & Peruzzo, P. (2010). Floating particle trapping and diffusion in vegetated open channel flow. *Water Resources Research*, *46*(11).

Defina, A., & Peruzzo, P. (2012). Diffusion of floating particles in flow through emergent vegetation: Further experimental investigation. *Water Resources Research*, *48*(3).

Defina, A., & Pradella, I. (2014). Vortex-induced cross-flow seiching in cylinder arrays. *Advances in water resources*, *71*, 140–148.

De Ryck, D. J., Robert, E. M., Schmitz, N., Van der Stocken, T., Di Nitto, D., Dahdouh-Guebas, F., & Koedam, N. (2012). Size does matter, but not only size: Two alternative dispersal strategies for viviparous mangrove propagules.

Aquatic botany, *103*, 66–73.

Dixon, K. R., & Florian Jr, J. D. (1993). Modeling mobility and effects of contaminants in wetlands. *Environmental Toxicology and Chemistry: An International Journal*, *12*(12), 2281–2292.

Fey, U., König, M., & Eckelmann, H. (1998). A new strouhal–reynolds-number relationship for the circular cylinder in the range 47< re< 2× 10 5. *Physics of Fluids*, *10*(7), 1547–1549.

Fischer, H., List, E., Koh, R., Imberger, J., & Brooks, N. (1979). Mixing in inland and coastal waters academic press. *New York*, 229–242.

Garcia, D., Obeso, J. R., & Martinez, I. (2005). Spatial concordance between seed rain and seedling establishment in bird-dispersed trees: does scale matter? *Journal of Ecology*, *93*(4), 693–704.

García, D., Rodríguez-Cabal, M. A., & Amico, G. C. (2009). Seed dispersal by a frugivorous marsupial shapes the spatial scale of a mistletoe population. *Journal of Ecology*, *97*(2), 217–229.

Griffith, A. B., & Forseth, I. N. (2002). Primary and secondary seed dispersal of a rare, tidal wetland annual, aeschynomene virginica. *Wetlands*, *22*(4), 696–704.

Groves, J. H., Williams, D. G., Caley, P., Norris, R. H., & Caitcheon, G. (2009). Modelling of floating seed dispersal in a fluvial environment. *River Research and Applications*, *25*(5), 582–592.

Ibáñez, I., Clark, J. S., Dietze, M. C., Feeley, K., Hersh, M., LaDeau, S., ... Wolosin, M. S. (2006). Predicting biodiversity change: outside the climate envelope, beyond the species–area curve. *Ecology*, *87*(8), 1896–1906.

Jordano, P., García, C., Godoy, J. A., & García-Castaño, J. L. (2007). Differential contribution of frugivores to complex seed dispersal patterns. *Proceedings of the National Academy of Sciences*, *104*(9), 3278–3282.

Kadlec, R. H. (1995). Overview: surface flow constructed wetlands. *Water Science and Technology*, *32*(3), 1–12.

Levine, J. M. (2003). A patch modeling approach to the community-level consequences of directional dispersal. *Ecology*, *84*(5), 1215–1224.

Liu, X., Zeng, Y., Katul, G., Huai, W., & Bai, Y. (2020). Longitudinal dispersal properties of floating seeds within open-channel flows covered by emergent vegetation. *Advances in Water Resources*, *144*, 103705.

MacLennan, A., & Vincent, J. (1982). Transport in the near aerodynamic wakes of flat plates. *Journal of Fluid Mechanics*, *120*, 185–197.

McDonald, K. (2014). *Tidal seed dispersal potential of spartina densiflora in humboldt bay (humboldt county, california)* (Unpublished master's thesis). Humboldt State University.

Mitsch, W. J., Gosselink, J. G., Zhang, L., & Anderson, C. J. (2009). *Wetland ecosystems*. John Wiley & Sons.

Nathan, R. (2006). Long-distance dispersal of plants. *Science*, *313*(5788), 786–788.

Nathan, R., & Muller-Landau, H. C. (2000). Spatial patterns of seed dispersal, their determinants and consequences for recruitment. *Trends in ecology & evolution*, *15*(7), 278–285.

Neff, K. P., & Baldwin, A. H. (2005). Seed dispersal into wetlands: techniques and results for a restored tidal freshwater marsh. *Wetlands*, *25*(2), 392–404.

Nepf, H. (1999). Drag, turbulence, and diffusion in flow through emergent vegetation. *Water resources research*, *35*(2), 479–489.

Nepf, H., Mugnier, C., & Zavistoski, R. (1997). The effects of vegetation on longitudinal dispersion. *Estuarine, Coastal and Shelf Science*, *44*(6), 675–684.

Nepf, H., Sullivan, J., & Zavistoski, R. (1997). A model for diffusion within emergent vegetation. *Limnology and Oceanography*, *42*(8), 1735–1745.

Nilsson, C., Brown, R. L., Jansson, R., & Merritt, D. M. (2010). The role of hydrochory in structuring riparian and wetland vegetation. *Biological Reviews*, *85*(4), 837–858.

Nilsson, C., Ekblad, A., Dynesius, M., Backe, S., Gardfjell, M., Carlberg, B., ... Jansson, R. (1994). A comparison of species richness and traits of riparian plants between a main river channel and its tributaries. *Journal of Ecology*, 281–295.

Nitto, D. D., Erftemeijer, P., Van Beek, J., Dahdouh-Guebas, F., Higazi, L., Quisthoudt, K., ... Koedam, N. (2013). Modelling drivers of mangrove propagule dispersal and restoration of abandoned shrimp farms. *Biogeosciences*, *10*(7), 5095–5113.

O'Reilly, C. M., Alin, S. R., Plisnier, P.-D., Cohen, A. S., & McKee, B. A. (2003). Climate change decreases aquatic ecosystem productivity of lake tanganyika, africa. *Nature*, *424*(6950), 766–768.

Orson, R. A., Simpson, R. L., & Good, R. E. (1992). A mechanism for the accumulation and retention of heavy metals in tidal freshwater marshes of the upper delaware river estuary. *Estuarine, Coastal and Shelf Science*, *34*(2), 171–186.

Palmer, M. R., Nepf, H. M., Pettersson, T. J., & Ackerman, J. D. (2004). Observations of particle capture on a cylindrical collector: Implications for particle accumulation and removal in aquatic systems. *Limnology and Oceanography*, *49*(1), 76–85.

Peruzzo, P., Defina, A., & Nepf, H. (2012). Capillary trapping of buoyant particles within regions of emergent vegetation. *Water Resources Research*, *48*(7).

Peruzzo, P., Defina, A., Nepf, H. M., & Stocker, R. (2013). Capillary interception of floating particles by surface-piercing vegetation. *Physical review letters*, *111*(16), 164501.

Peruzzo, P., Viero, D. P., & Defina, A. (2016). A semi-empirical model to predict the probability of capture of buoyant particles by a cylindrical collector through capillarity. *Advances in Water Resources*, *97*, 168–174.

Phillips, J. D. (1989). Fluvial sediment storage in wetlands 1. *JAWRA Journal of the American Water Resources Association*, *25*(4), 867–873.

Richards, S. A., Possingham, H. P., & Noye, B. (1995). Larval dispersion along a straight coast with tidal currents: complex distribution patterns from a simple model. *Marine Ecology Progress Series*, *122*, 59–71.

Rubenstein, D. I., & Koehl, M. A. (1977). The mechanisms of filter feeding: some theoretical considerations. *The American Naturalist*, *111*(981), 981–994.

Rutherford, J. C. (1994). *River mixing*. John Wiley & Son Limited.

Schupp, E. W., Jordano, P., & Gómez, J. M. (2010). Seed dispersal effectiveness revisited: a conceptual review. *New Phytologist*, *188*(2), 333–353.

Shi, W., Peruzzo, P., & Defina, A. (2021). An eulerian model for the transport and diffusion of floating particles within regions of emergent vegetation. *Water Resources Research*, e2021WR029625.

Shi, W., Shao, D., Gualtieri, C., Purnama, A., & Cui, B. (2020). Modelling long-distance floating seed dispersal in salt marsh tidal channels. *Ecohydrology*, *13*(1), e2157.

Shucksmith, J., Boxall, J., & Guymer, I. (2011). Determining longitudinal dispersion coefficients for submerged vegetated flow. *Water Resources Research*, *47*(10).

Sousa, W. P., Kennedy, P. G., Mitchell, B. J., & Ordóñez L, B. M. (2007). Supply-side ecology in mangroves: do propagule dispersal and seedling establishment explain forest structure? *Ecological Monographs*, *77*(1), 53–76.

Spiegel, O., & Nathan, R. (2007). Incorporating dispersal distance into the disperser effectiveness framework: frugivorous birds provide complementary dispersal to plants in a patchy environment. *Ecology letters*, *10*(8), 718–728.

Tanino, Y., & Nepf, H. M. (2008). Laboratory investigation of mean drag in a random array of rigid, emergent cylinders. *Journal of Hydraulic Engineering*, *134*(1), 34–41.

Van der Stocken, T., De Ryck, D. J., Vanschoenwinkel, B., Deboelpaep, E., Bouma, T. J., Dahdouh-Guebas, F., & Koedam, N. (2015). Impact of landscape structure on propagule dispersal in mangrove forests. *Marine Ecology Progress Series*, *524*, 95–106.

Van der Stocken, T., Vanschoenwinkel, B., De Ryck, D. J., Bouma, T. J., Dahdouh-Guebas, F., & Koedam, N. (2015). Interaction between water and wind as a driver of passive dispersal in mangroves. *PLoS One*, *10*(3), e0121593.

Vella, D., & Mahadevan, L. (2005). The "cheerios effect". *American journal of physics*, *73*(9), 817–825.

Viero, D. P., Pradella, I., & Defina, A. (2017). Free surface waves induced by

vortex shedding in cylinder arrays. *Journal of Hydraulic Research*, *55*(1), 16–26.

White, B. L., & Nepf, H. M. (2003). Scalar transport in random cylinder arrays at moderate reynolds number. *Journal of Fluid Mechanics*, *487*, 43.

Yuhong, Z., & Xi, Z. (2017). Review on seeds floating and settling kinetic characteristics dispersed by hydrochory. *Yangtze River*, *48*(17), 20.

Yusuf, B., Karim, O., & Osman, S. (2009). Numerical solution for open channel flow with submerged flexible vegetation. *Int. J. Eng. Tech*, *61*, 39–50.

Ziada, S. (2006). Vorticity shedding and acoustic resonance in tube bundles. *Journal of the Brazilian Society of Mechanical Sciences and Engineering*, *28*, 186–189.

Appendix

A Derivation of c

On writing

$$c = c_1 \exp(-\varphi t), \tag{A.1}$$

the equation 2.1 reduces to

$$\frac{\partial c_1}{\partial t} + U_m \frac{\partial c_1}{\partial x} = D \frac{\partial^2 c_1}{\partial x^2}. \tag{A.2}$$

Transforming the fixed coordinate into a moving coordinate system with constant velocity U_m,

$$\theta = x - U_m t, \tag{A.3}$$

we obtain

$$\frac{\partial c_1}{\partial t} = D \frac{\partial^2 c_1}{\partial \theta^2}. \tag{A.4}$$

The initial and boundary conditions become $c_1(\theta, 0) = \delta(\theta), c_1(\pm\infty, t) = 0$, as such, we can obtain the solution of the pure diffusion equation as

$$c_1(\theta, t) = \frac{1}{\sqrt{4\pi D t}} \exp[-\frac{\theta^2}{4Dt}]. \tag{A.5}$$

Substituting the equation A.1 and A.3 into A.5, we can yield the solution of Equation 2.1 as below

$$c(x,t) = \frac{1}{\sqrt{4\pi Dt}}\exp[-\frac{(x-U_m t)^2}{4Dt} - \varphi t]. \tag{A.6}$$

B Derivation of c_p

On writing

$$c = c_2 \exp(-\varphi t), \tag{B.1}$$

the equation 2.8 reduces to

$$\frac{\partial c_2}{\partial t} + U\frac{\partial c_2}{\partial x} = 0. \tag{B.2}$$

The prototypical solution of 1D advection only equation is

$$c_2 = \delta(x - Ut), \tag{B.3}$$

with Dirac delta function $\delta(x)$ as the initial condition. Substituting the equation B.1 into B.3, we obtain the solution of equation 2.8 as

$$c = e^{-\varphi t}\delta(x - Ut). \tag{B.4}$$

Thus we can write the equation 2.2 as

$$\frac{\partial c_p}{\partial c} = \varphi e^{-\varphi t}\delta(x - Ut). \tag{B.5}$$

Applying Laplace transformation to equation B.5 gives:

$$L\{\frac{\partial c_p}{\partial t}\} = L\{\varphi e^{-\varphi t}\delta(x - Ut)\}. \tag{B.6}$$

The left term of equation B.6 is

$$L\{\frac{\partial c_p}{\partial t}\} = sL\{c_p\} - c_p(0) = sL\{c_p\}, \tag{B.7}$$

as $c_p(0) = 0$. And the right term of equation B.6 equals

$$\int_{0^-}^{+\infty} \varphi e^{-(s+\varphi)t}\delta(x - Ut)\, dt = \int_{-\infty}^{+\infty} \varphi e^{-(s+\varphi)t}\delta(x - Ut)\, dt. \tag{B.8}$$

According to the proporties of Dirac Delta function that,

$$\int_{-\infty}^{+\infty} f(x)\delta(x)\, dx = f(0), \tag{B.9}$$

and by applying $(x - Ut) = t^*$, we can finally obtain the solution of the right term of equation B.6 as

$$L\{\varphi e^{-\varphi t}\delta(x - Ut)\} = \frac{\varphi}{U} e^{-(s+\varphi)x/U}. \tag{B.10}$$

Thus,

$$sL\{c_p\} = \frac{\varphi}{U} e^{-(s+\varphi)x/U}. \tag{B.11}$$

By taking the inverse Laplace transformation of equation B.11, we can obtain the solution of equation B.5 as

$$c_p = \frac{\varphi}{U} e^{-\varphi x/U} H(t - \frac{x}{U}). \tag{B.12}$$

Equivalently, it can be rewritten as

$$c_p(x,t) = \begin{cases} \frac{\varphi}{U} e^{-\varphi x/U} & x \leq Ut \\ 0 & x > Ut \end{cases} . \tag{B.13}$$

C Correction of T

We have known that t_{obs} is the observation time (i.e. 600s in this study), T is the mean residence time, T_{obs} is the mean time of all the temporary trapping events whose time is less than t_{obs}.

The distribution of residence times τ is actually the truncated exponential distribution, $p_{trunc}(\tau)$, i.e.

$$p_{trunc}(\tau) = \begin{cases} ke^{-\tau/T} & \tau \leq t_{obs} \\ 0 & \tau > t_{obs} \end{cases} . \tag{C.1}$$

Since we know that

$$\int_0^\infty p_{trunc}(\tau)\, d\tau = 1, \tag{C.2}$$

then we have

$$1 = \int_0^\infty p_{trunc}(\tau)\, d\tau = \int_0^{t_{obs}} ke^{-\tau/T} d\tau + \int_{t_{obs}}^\infty 0 d\tau = kT(1 - e^{-t_{obs}/T}). \tag{C.3}$$

Hence we can obtain that

$$k = \frac{1}{T(1 - e^{-t_{obs}/T})}. \tag{C.4}$$

Subscribing the equation C.4 into equation C.1, the equation C.1 can be rewritten as

$$p_{trunc}(\tau) = \begin{cases} \frac{\frac{1}{T}e^{-\tau/T}}{1-e^{-t_{obs}/T}} & \tau \leq t_{obs} \\ 0 & \tau > t_{obs} \end{cases} , \tag{C.5}$$

and the mean time of all temporary trapping events whose time is less than t_{obs}, T_{obs}, as the expected value of the truncated exponential distribution, reads as be-

low

$$T_{obs} = \int_0^{\infty} \tau p_{trunc}(\tau) d\tau = \int_0^{t_{obs}} \tau \frac{\frac{1}{T} e^{-\tau/T}}{1 - e^{-t_{obs}/T}} d\tau = \frac{\int_0^{t_{obs}} \tau \frac{1}{T} e^{-\tau/T} d\tau}{1 - e^{-t_{obs}/T}}. \quad \text{(C.6)}$$

As

$$p(\tau) = \frac{1}{T} e^{-\tau/T}, \quad \text{(C.7)}$$

and

$$1 - e^{-t_{obs}/T} = \int_0^{t_{obs}} p(\tau) d\tau, \quad \text{(C.8)}$$

therefore, the equation C.6 can be written as

$$T_{obs} = \frac{\int_0^{t_{obs}} \tau p(\tau) d\tau}{\int_0^{t_{obs}} p(\tau) d\tau}, \quad \text{(C.9)}$$

which is exactly the equation 3.5 in Chapter 3.

D Derivation of P_t and P_c

As we know, N_t is the observed number of the long-time retention events with retention time τ shorter than t_{obs}, N_c is the observed number of the capture events with retention time τ larger than t_{obs}, N_i is the total number of the observed particle-stem interactions.

Let N_t' be the actual number of the long-time retention events, N_c is the actual number of permanent capture events. Thus we can write

$$N_t + N_c = N_t' + N_c' = M. \tag{D.1}$$

As we have assumed that $P(\tau > t)$ is

$$P(\tau > t) = (1 - A)e^{-t/T} + A, \tag{D.2}$$

with

$$A = \frac{P_c}{P_c + P_t} = \frac{N_c'}{N_c' + N_t'} = \frac{M - N_t'}{M} = 1 - \frac{N_t'}{M}, \tag{D.3}$$

so when $t = t_{obs}$, we have

$$P(\tau > t_{obs}) = (1 - A)e^{-t_{obs}/T} + A = \frac{N_c}{M}, \tag{D.4}$$

and hence

$$A = 1 - \frac{N_t}{(1 - e^{-t_{obs}/T})M}. \tag{D.5}$$

Combining equation D.3 with D.5, we can obtain

$$N_t' = \frac{N_t}{(1 - e^{-t_{obs}/T})}, \tag{D.6}$$

thus we can obtain the probability that a particle remains trapped for a long time

P_t as

$$P_t = \frac{N_t'}{N_i} = \frac{N_t}{(1 - e^{-t_{obs}/T})N_i}, \tag{D.7}$$

and the probability that a particle remains permanently captured P_c can be obtained as

$$P_c = \frac{N_c'}{N_i} = \frac{N_t + N_c - N_t'}{N_i} = \frac{N_c}{N_i} + P_t(1 - e^{-t_{obs}/T}) - P_t = \frac{N_c}{N_i} - P_t e^{-t_{obs}/T} \tag{D.8}$$